Universiteit Utrecht

Koninklijk Nederlands Meteorologisch Instituut
Ministerie van Infrastructuur en Waterstaat

Long-Term Wind Influence on Sea-Level Change Along the Dutch Coast

Master Thesis

Climate Physics

Iris J. Keizer

Supervisors:

Dr. D. Le Bars
Royal Netherlands Meteorological Institute (KNMI)

Prof. Dr. R. S. W. van de Wal
Institute for Marine and Atmospheric Research, Utrecht University
Department of Physical Geography, Utrecht University

Prof. Dr. S. S. Drijfhout
Royal Netherlands Meteorological Institute (KNMI)
Institute for Marine and Atmospheric Research, Utrecht University

January 2022

Abstract

The sea level along the Dutch coast contains a robust interannual variability, of which a substantial part is due to wind forcing. Correcting sea level observations for the wind influence helps to improve estimates of long-term rates of sea-level rise. We study the wind influence on multi-decadal sea-level variability and trend along the Dutch coast by using three physically-based, multi-linear regression models. These models relate sea level and wind forcing either using zonal and meridional wind speeds or large-scale pressure patterns. We use annual mean sea level observations from six tide gauge stations spread along the Dutch coast covering 1890 to 2020, and surface wind and pressure data from the ERA5 and the Twentieth Century Reanalysis data sets, covering 1950 to 2020 and 1836 to 2015, respectively. The results from the regression analysis show a robust multi-decadal variability of wind influence on sea-level change with an amplitude of around 1 cm and a period of 40 to 60 years. This multi-decadal mode of variability is responsible for an average drop in sea level of 0.5 mm/yr over the last 40 years. Furthermore, it is shown that the multi-decadal wind variability is related to the Atlantic Multidecadal Variability (AMV). A regression analysis relating the low-frequency variability and AMV from 1950 to 2015 shows that the AMV explains a large part of the wind variability. Finally, the three regression models are applied to Coupled Model Intercomparison Project 6 (CMIP6) historical and future climate scenario data to make projections of the wind impact on sea-level change along the Dutch coast for the 21st century. We do not find significant effects of wind on sea-level rise for the Dutch coast during the 21st century, which contrasts earlier findings for the German Bight.

Plain Language Summary

Global mean sea levels are rising. The main cause of sea-level rise since the industrial revolution is global warming due to greenhouse gas emissions caused by human activity. As a result of global warming, ocean temperatures are increasing, causing the volume of oceans to increase as well. Also, ice masses around the globe are melting, and meltwater ends up in the oceans. Due to these processes and others, over the last century, global mean sea level has risen faster than in any century since late prehistory. Measurements show that the rate of global mean sea-level rise has been accelerating since the late 1960s and is expected to further accelerate throughout the 21st century. Since the North Sea is connected to the global oceans, an acceleration of sea-level rise is also expected to be measured along the Dutch coast. However, on a regional scale, sea-level changes can depart from the global mean due to mechanisms of which the impact vanishes when you take a global average. Also, annual sea level measurements along the Dutch coast show a large interannual variability partly driven by wind forcing. This large variability makes estimates of changing rates of sea-level rise harder to detect. Therefore, understanding the influence of the wind effect on sea-level changes helps to correct the sea level measurements for some of the interannual variability and thereby can help to detect an acceleration of sea-level rise. We focus on the multi-decadal wind influence over a long period of almost two centuries.

The wind impacts sea level because it exerts a stress force on the water surface by blowing over it, which causes the transport of water masses. The effect of this wind forcing is more significant for shallower water masses. Since the North and Wadden Sea are relatively shallow, wind forcing substantially impacts sea-level changes along the Dutch coast. Along the Dutch coast, the highest sea levels are caused by north-westerly winds. The number and strength of storms as well as consistent north-westerly winds can impact annual sea level by 10 cm.

We find a structural trend in the wind influence on sea-level changes of about 0.1-0.3 mm/yr since 1836. However, on shorter time scales of several decades, the wind influence shows a multidecadal variability with an amplitude of 1 cm and a period of 40 to 60 years. This means that over some decades, the wind raised sea level by 1.0 mm/yr and for other decades, the wind dropped sea level by 0.5 mm/yr, which happened between 1980 and 2020. This negative wind effect on sea level occurred when global mean sea levels were accelerating. Removing the effect of the wind from sea level measurements also shows an acceleration of sea-level rise along the Dutch coast. The negative wind impact that we see for recent decades thus played an important role in masking the acceleration of sea-level rise along the Dutch coast.

As a next step, we investigated whether we could find large-scale drivers of the multidecadal variability in the wind influence on sea-level changes. We focus on the Atlantic Multidecadal Variability (AMV), a known pattern of multidecadal sea surface temperature (SST) variability. The AMV is an important driver of multidecadal climate variability in the North Atlantic region. Therefore, it's interesting to study its influence on the multidecadal variability of wind influence on sea-level changes along the Dutch coast. We find that the AMV is indeed an essential driver of the wind-driven multidecadal sea-level variability. The AMV is a large-scale phenomenon constructed from sea surface temperature (SST) measurements. To better understand its connection to the wind-driven sea-level variability, we also study the influence of SST measurements from the North Atlantic region on the wind-driven sea-level variability. We can link SST measurements to the wind-driven sea-level variability for some regions. These regions include the Northern waters around Greenland, including the Labrador, Irminger, and the Greenland Sea, and waters along the east coast of America, including the Caribbean Sea.

Finally, we investigated what can be expected of wind-driven sea-level changes for the 21st century. We first performed the same analysis between wind and sea-level changes over the historical period using climate model data. The results show that some climate models can reproduce the wind-driven sea-level variability. These climate models are used to project the wind influence on sea-level changes for the 21st century. Our results show that the natural variability of the wind effect on sea-level changes continues throughout the 21st century with an amplitude of 1 cm. The climate models cannot reproduce the linear trend we found for the wind influence over the historical period. Also, no significant trend is found for the wind influence for the 21st century.

In this study, we thus found that, over past centuries, the wind influence on sea-level changes was dominated by natural variability that we can link to the AMV. Over recent decades the wind tended to decrease sea level, thereby masking an acceleration of sea-level rise along the Dutch coast. Since this drop in sea level was caused by natural variability, which is expected to continue throughout the 21st century, future sea-level rise will catch up from this drop, and we expect to see a further acceleration of sea level along the Dutch coast.

Contents

1 Introduction

Rising sea levels are an essential indicator and well-known consequence of global warming resulting from anthropogenic greenhouse gas (GHG) emissions [Slangen, Church, et al. 2016; Fox-Kemper et al. 2021]. Global mean sea level (GMSL) has risen during the 20th century at an accelerated rate and is expected to continue to rise at an accelerated rate throughout the 21st century [Fox-Kemper et al. 2021; Church and White 2011; Dangendorf, Marcos, et al. 2017; Gehrels and Woodworth 2013; Kopp et al. 2016; Meyssignac and Cazenave 2012; Slangen, van de Wal, et al. 2014; Wöppelmann et al. 2009]. The rising ocean levels have a broad socio-economic and environmental impact on coastal zones and communities around the world, especially for low-lying countries like the Netherlands [Hinkel et al. 2014; Nauels et al. 2017; Nicholls et al. 2019]. In the Netherlands, sea-level rise threatens almost a third of the land which is located below the sea level of the North and Wadden Sea [van Koningsveld et al. 2008]. This is an essential social and economic region where 9 million people live and 70% of the gross domestic product is earned. In addition, sea-level rise is a threat for vulnerable regions like the Wadden Sea World Heritage area, where even small external changes may disturb the ecosystem's delicate equilibrium [Vermeersen et al. 2018; Kirwan and Megonigal 2013]. Hence, making reliable projections of future sea-level rise is crucial to make the best mitigation and adaptation decisions.

The recent sixth assessment report (AR6) of the Intergovernmental Panel on Climate Change (IPCC) [Fox-Kemper et al. 2021] shows that GMSL rose 20 [15-25] cm over the period from 1901 to 2018 with a corresponding rate of 1.7 mm/yr which was faster than in any prior century over the last three millennia. Observations of GMSL are shown by the orange and purple lines in Figure 1. These observations show that GMSL rise has accelerated since the late 1960s. The AR6 report indicates that GMSL is expected to accelerate throughout the 21st century. GMSL rise is the net result of many individual geophysical and climatological processes of which the main contributors are ocean thermal expansion, mass loss from glaciers, and mass loss from ice sheets [Fox-Kemper et al. 2021; Frederikse et al. 2020; Vermeersen et al. 2018]. The GMSL rise and its major constituents are depicted in Fig 1.

Sea levels along the Dutch coast are monitored using a network of tide gauges and satellite altimetry which is analyzed and explained to policymakers by the Zeespiegelmonitor, published by Deltares [Baart, Rongen, et al. 2019]. The Zeespiegelmonitor shows that since 1901 sea-level rise along the Dutch coast rose 22 cm, close to the globally observed average. On regional scales, mean sea-level changes can depart from GMSL rise [Meyssignac, Slangen, et al. 2017; Fox-Kemper et al. 2021; Church and White 2011; Meyssignac and Cazenave 2012; Ray and Douglas 2011; Douglas 1992] For the Dutch coast, regional differences are caused by vertical land motion, water temperature, salinity, air pressure, wind forcing, and changes in the Earth's gravitational field due to mass loss from ice sheets. For instance, a quarter of the sea-level rise along the Dutch coast over the past century was due to subsidence. The regional differences caused by these processes vanish when the global average is obtained. For the sea level observations along the Dutch coast, these processes also result in a more considerable interannual variability, as can be seen in Fig. 1. Due to this large interannual variability, detecting an acceleration of sea-level rise is harder. However, since the North Sea is connected to global ocean waters, the acceleration of sea-level rise is also expected to be measured along the Dutch coast. We know that a large part of the sea-level variability along the Dutch coast is caused by wind forcing. Wind blowing over a water surface can influence coastal sea level since it exerts a stress force on the water surface, leading to water transport. For the Dutch coast, north-westerly winds induce the most considerable sea-level changes. Wind forcing leads to higher surges for shallower seas. Since the North and Wadden sea are relatively shallow seas with average depths of respectively 90 and 10 m, wind forcing can influence annual sea-level changes of 6 cm standard deviation. Large differences can be caused by the occurrence and strength of both consistent northwestern winds and storms.

In this thesis, we study the long-term wind influence on sea-level changes as these results can help to detect an acceleration of sea-level rise. In addition, a preliminary budget analysis of contributions to sea-level rise along the Dutch coast showed that wind had the influence to drop sea level by 0.5 mm/yr over the period from 1979 to 2018. Therefore, we want to know if the wind dropped sea level over recent decades and whether this might mask a possible acceleration of sea-level rise. Additionally, it is essential to understand whether this drop was caused by natural variability and future sea levels might catch up from this drop or whether it was due to a structural change that might protect the Dutch coast from a fraction of future sea-level rise. Using three multiple linear regression models, the long-term wind influence on sea-level change along the Dutch coast.

When the wind influence on sea-level changes is obtained, we study whether we can identify large-scale drivers of the wind-driven sea-level variability. The Atlantic Multidecadal Variability (AMV) is a multi-decadal mode of sea surface temperature (SST) variability in the North Atlantic Ocean. The AMV is an important driver of decadal climate variability in the North Atlantic region. Therefore, we study the influence of the AMV on wind-driven sea-level variability. Additionally, we also study the influence of local SST in the North Atlantic

region on wind-driven sea-level variability. Thereby we aim to better understand which regions of SST in the North Atlantic Ocean influence wind-driven sea-level variability along the Dutch coast. Again, we use linear regression for these analyses.

As a final step, we study what we can expect of the wind influence for the 21st century. We perform the same regression analysis between wind and sea-level data over the historical period as for the observations. However, we now use climate model data from the Coupled Model Intercomparison Project 6 (CMIP6). The regression results using climate model data are compared to the regression results using observations. Climate models that can show similar results as we found for the observations are then used to make projections for the 21st century.

To summarize, in this study we aim to answer the following research questions:

1. *What was the wind influence on sea-level change along the Dutch coast over the historical period?*
2. *Can we identify large-scale drivers of the wind-driven sea-level variability?*
3. *What can be expected of the wind influence for the 21st century?*

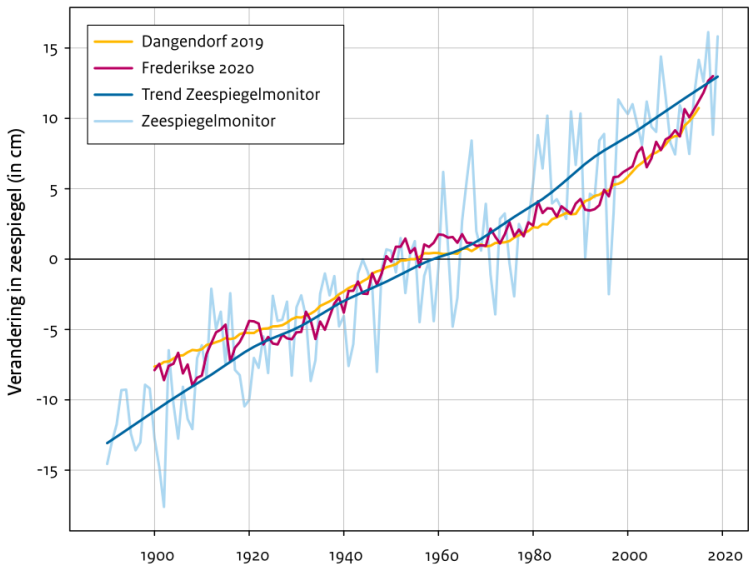

Figure 1: Observed global mean sea level, shown by the orange [Dangendorf, Hay, et al. 2019] and purple [Frederikse et al. 2020] lines and observed sea level along the Dutch coast, shown by the blue line [Baart, Rongen, et al. 2019]. The figure is obtained from KNMI's Klimaatsignaal'21 [KNMI 2021].

2 Data

2.1 Observational and Reanalysis Data

2.1.1 Sea Level Height Observations

We use annual sea level height measurements from 6 tide gauges along the Dutch coast to study the wind influence on sea-level changes. These measurements are provided by the Permanent Service for Mean Sea Level and are adjusted to the Revised Local Reference datum [PSMSL 2021; Holgate et al. 2013]. We use the same 6 tide gauge stations were used in the Zeespiegelmonitor: Delfzijl, Den Helder, Harlingen, IJmuiden, Hoek van Holland and Vlissingen (Baart, Rongen, et al. 2019). Tide gauges are measurement tools that have sensors to measure the height of the surrounding sea level, which they do relative to a benchmark on nearby land. Therefore the measured sea level height is called relative sea level (RSL). As a vertical motion of land will result in a measured sea-level change, the measurements are corrected for vertical land motion by using predictions of vertical land movement and the Global Navigation Satellite Systems (GNSS) [Holgate et al. 2013]. The tide gauge observations have a long temporal coverage and are uniformly distributed along the Dutch coast. While the time series for the different stations start between 1862 and 1872, only the data from 1890 to 2020 is used for the analysis. We obtain anomalies of the observations over the given period. The data will be referred to as relative sea-level change (RSLC).

Both the 18.6 yr lunar nodal cycle and the inverse barometer effect (IBE) can play an important factor in the decadal variability of regional sea level [Baart, van Gelder, et al. 2012; Stammer and Höttemann 2008]. Therefore, we correct the RSLC data by removing their contribution to sea-level changes. The influence of the nodal cycle is obtained using the method described in [Hermans et al. 2020; Woodworth 2012]. For each latitude λ of a given tide gauge station and for each year t, the nodal correction is given by:

$$A = 0.44(1 + 0.298 - 0.6032) \cdot 20 \cdot \left(3\sin^2\lambda - 1\right) \tag{1}$$

$$\text{nodal correction} = A \cdot \cos\left(\frac{2\pi \cdot (t - 1922.7)}{18.61} + \pi\right) \tag{2}$$

The influence of the nodal cycle on sea-level changes is minor, as can be seen in Fig. 2a where the non-corrected tide gauge data and the tide gauge data corrected for the nodal cycle are shown for Hoek van Holland. Using the equations above, we find that the amplitude of the nodal cycle varies between 0.5 and 0.6 cm for the different tide gauge stations. The inverted barometer response to local RSLC can be expressed as:

$$\eta(t) = -\frac{p_a(t)}{\rho_0 g} \tag{3}$$

where p_a is the atmospheric pressure, $\rho_0 = 1030\,\text{kg/m}^3$ is the water density and g is the local gravitational acceleration Piecuch, Thompson, and Donohue 2016; Stammer and Höttemann 2008; Jeffreys 1916; Wunsch and Stammer 1997. To obtain the IB response, reanalysis pressure data is used. Values near the tide gauge station are selected, whereof time anomalies are obtained. After that, the IB response for each tide gauge station is calculated using equation 3, of which again anomalies are obtained. A plot of the tide gauge record for Hoek van Holland corrected for the IBE can is shown in Fig. 2a. The IBE has a standard deviation of 1.3 cm and reaches maximum values between 4.3 and 4.7 cm for the different tide gauges stations. After the tide gauge data is corrected for the nodal cycle and the inverse barometer effect for the data from each tide gauge station, also the average of the different stations is obtained and used for analysis. The resulting tide gauge data that is used in further research is shown in Fig. 2b.

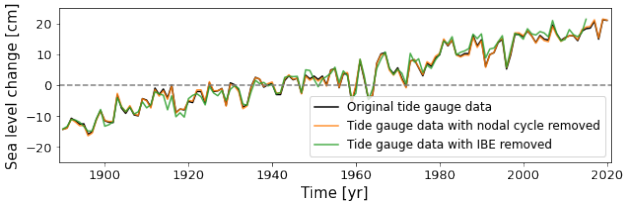

(a) Annual tide gauge relative sea-level change for Hoek van Holland. Data without applying a correction and corrected for the nodal cycle or the inverse barometer effect is shown.

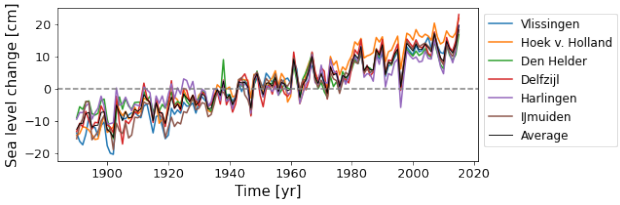

(b) Annual tide gauge relative sea-level change for six different tide gauge stations and their average. The tidal nodal cycle and inverse barotropic effect have been removed from the time series.

Figure 2: Observational sea level height data from different tide gauge stations along the Dutch coast.

2.1.2 Atmospheric Reanalysis Data

We use atmospheric data fields from two reanalysis products to study the wind influence. First, monthly averaged data on single levels from the ERA5 reanalysis (ERA5) from the Copernicus Climate Change service Climate Data Store is used [Hersbach, Bell, and Berrisford 2021]. The ERA5 reanalysis data has a spatial resolution of 0.25°×0.25° and we use data from 1960 to 2020. The data over this period consists of a data set over the period from 1979 to the present (Hersbach, Bell, and Berrisford 2021) and a preliminary data set over the period from 1950 to 1978 [Bell et al. 2021]. The latter data set is called preliminary as it suffers from some unrealistic behaviour, tropical cyclones are sometimes too intense, compared to the data set over the more recent period [Bell et al. 2021; Hersbach, Bell, Berrisford, et al. 2020]. To establish the wind influence on RSLC, wind stress forcing and sea level pressure fields are analysed. Therefore, we use 10 m zonal and meridional wind speed and mean sea level pressure.

Second, the Twentieth Century Reanalysis Version 3 (20CRv3) from the National Oceanographic and Atmospheric Administration (NOAA) is used [PSL 2021]. Also, monthly averaged data on single levels is used. The data covers 1836 to 2015 and has a spatial resolution of 1.0°×1.0°. We use the same variables as for the ERA5 reanalysis data set.

2.1.3 Sea Surface Temperature Data

Also, the influence of sea surface temperature on wind-driven sea-level variability is studied. For this, two different data sets from the NOAA are used. From the 20CRv3 data set, the monthly averaged skin temperature at the surface is used [PSL 2021]. Second, monthly averaged data from the Extended Reconstructed Sea Surface Temperature V5 (ERSSTv5) is used [Huang et al. 2017]. This data set has a spatial resolution of 2.0°×2.0° and we use data from 1854 to 2020. We obtain annual averages to use for the analysis.

Three AMV records were used to study the influence of the Atlantic Multidecadal Variability (AMV) on the atmospheric contribution to sea level. The monthly averaged data is taken over the region 0°N to 60°N and 80°W to 0°E and has been deseasonalised and detrended as described in [Jüling, von der Heydt, and Dijkstra 2021]. The AMV records are obtained using three data sets from sea surface temperature observations. First, the Hadley Centre Sea Ice and Sea Surface Temperature dataset (HadISST) extending from 1870 to 2018 is used [Rayner et al. 2003]. Further, the COBE-SST2 and the ERSSTv5 data sets from NOAA are used and are used for the same period [Hirahara, Ishii, and Fukuda 2014; Huang et al. 2017]. All data sets have a spatial resolution of 1.0°×1.0°.

2.2 CMIP6 Model Data

To study the wind influence on sea-level changes for the 21st century, we use data from climate models from the Coupled Model Intercomparison Project 6 (CMIP6). We use CMIP6 historical simulations to compare the results of the climate models to observations. The historical simulations run from 1850 to 2014 and the projections from 2015 to 2100. Three Shared Socioeconomic Pathways (SSPs or scenarios) are used for the projections. Scenarios are connected to pathways of future radiative forcing known as Representative Concentration Pathways (RCP). The used scenarios lead to low radiative forcing (SSP1-RCP2.6), intermediate forcing (SSP2-RCP4.5) and high forcing (SSP5-RCP8.5) [van Vuuren et al. 2011]. The climate model data has a grid size of 1.0°×1.0°. For the analysis, we use annual mean dynamic sea level above the geoid, annual zonal and meridional 10 m wind speed and annual air pressure at sea level. The dynamic sea level does not include the inverse barometer effect [Stammer and Höttemann 2008]. The dynamic sea level data is plotted for a selection of models in Fig. 3. Climate models are chosen that are available for all variables, scenarios, and periods, including 28 models from 17 modelling centres. The used models are given in Appendix Sect. D.

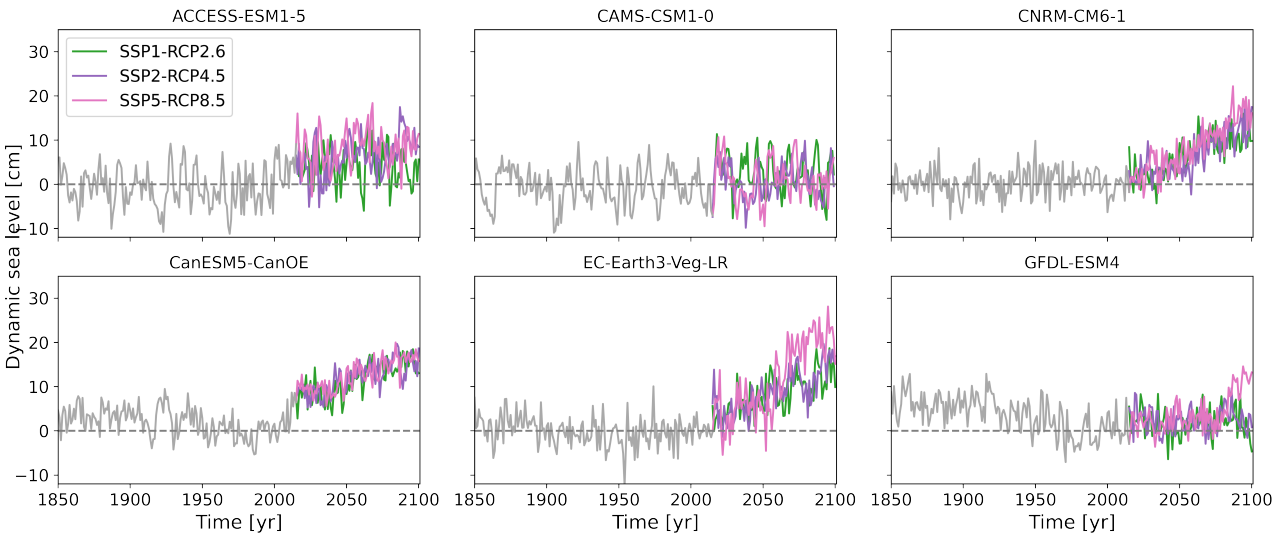

Figure 3: Plots of the annual dynamic sea level over from 1850 to 2100 for some of the models that are bold in Tab. 6

3 Methods

3.1 The Wind Influence on Sea-Level Change over the Historical Period using Observations

The long-term wind influence on sea-level change is analysed using three different multiple linear regression models, referred to as the NearestPoint, Timmerman and Dangendorf regression models. Using three different models reduces arbitrary methodological choices that might arise from using a single method. The three regression models reconstruct observed annual sea level anomalies from the 6 tide gauge stations and their average. Therefore, the annual time series of RSLC are used as the dependent variable in the regression models. Each regression model uses different forcing parameters to find the wind influence on RSLC. The analyses are performed using the atmospheric data from both the ERA5 and 20CRv3 reanalysis data sets. The regression analysis is performed over the overlapping period of sea level and wind data, using ERA5 from 1950 to 2020 and using 20CRv3 from 1890 to 2015. However, for comparison of the different reanalysis products and the climate model data, the analysis is also performed over the overlapping period from 1950 to 2014. Estimates of the linear trend also depend on the analysed period. Therefore, performing the analysis for the overlapping period allows making a good comparison between results of the linear trend for different reanalysis data sets and climate model data. The following section explains the multiple linear regression method, after that, the three regression models that are used in the analysis are presented, and finally, it is discussed how we analyse the results of the regression analyses and the performance of the different regression models.

3.1.1 Multiple Linear Regression

A multiple linear regression model estimates the relationship between a dependent variable (y) and multiple explanatory variables (x_1, x_2, ..., x_n) [Tranmer and Elliot 2008; Thomson and Emery 2014]. The multiple linear regression model described here is an ordinary least squares linear regression. It is called linear as the dependent variable is expected to be related to a linear combination of the explanatory variables. If the variables are time series, the model can be expressed as:

$$y(t) = \alpha + \beta_1 \cdot x_1(t) + \beta_2 \cdot x_2(t) + ... + \beta_n \cdot x_n(t) + \epsilon(t). \tag{4}$$

Here, α is a constant, $\epsilon(t)$ is an error term for each time step and β_1 till β_n are the regression coefficients that represent the influence of each explanatory variable on the dependent variable. [Heij et al. 2004].

An advantage of using regression models over more advanced but accurate models like coupled barotropic or baroclinic ocean-atmosphere models is that they are computationally cheap. This makes the use of regression models well suited for the study where many different aspects are studied.

We include the trend as an explanatory variable in each regression model in our analysis. Each model in our analysis thus includes:

$$\eta(t) = \alpha + \beta_{\mathrm{tr}} \cdot \mathrm{tr}(t) + ... + \epsilon(t) \tag{5}$$

where $\eta(t)$ is the RSLC and $\mathrm{tr}(t)$ denotes the trend and β_{tr} its regression coefficient. The trend is a linear series of numbers from zero to the period length. We include the trend in the regression to separate the long-term structural change caused by wind forcing from the long-term structural change caused by other mechanisms. A similar method was applied in the Zeespiegelmonitor [Baart, Rongen, et al. 2019].

3.1.2 NearestPoint Regression Model

Of the three regression models, the NearestPoint model is based on the approach used in the Zeespiegelmonitor [Baart, Rongen, et al. 2019]. It uses local wind speed measurements to parametrise zonal and meridional wind forcing as explanatory variables in the regression with RSLC. In the NearestPoint regression model, for the location of each tide gauge station, the nearest wind observations above the North or Wadden sea are selected. The locations whereof wind speed measurements are obtained are shown in Fig. 4a. The local 10 m zonal and meridional wind velocities are used to represent the wind forcing by multiplying their values with the absolute value, and the resulting time series are shown in Fig. 5. In the NearestPoint regression model, the RSLC is thus reconstructed using the zonal and meridional wind forcing and, as described before, the trend caused by other processes than wind forcing. For each tide gauge station, the reconstructed RSLC can thus be expressed as:

$$\eta(t) = \alpha + \beta_{\mathrm{tr}} \cdot \mathrm{tr}(t) + \underline{\beta_u \cdot U(t)|U(t)| + \beta_v \cdot V(t)|V(t)|} + \epsilon(t). \tag{6}$$

Each β indicates a resulting regression coefficient, and tr represents the trend, and $U(t)|U(t)|$ and $V(t)|V(t)|$ are the parametrisations of the zonal and meridional wind forcing nearby the tide gauge station. Additionally,

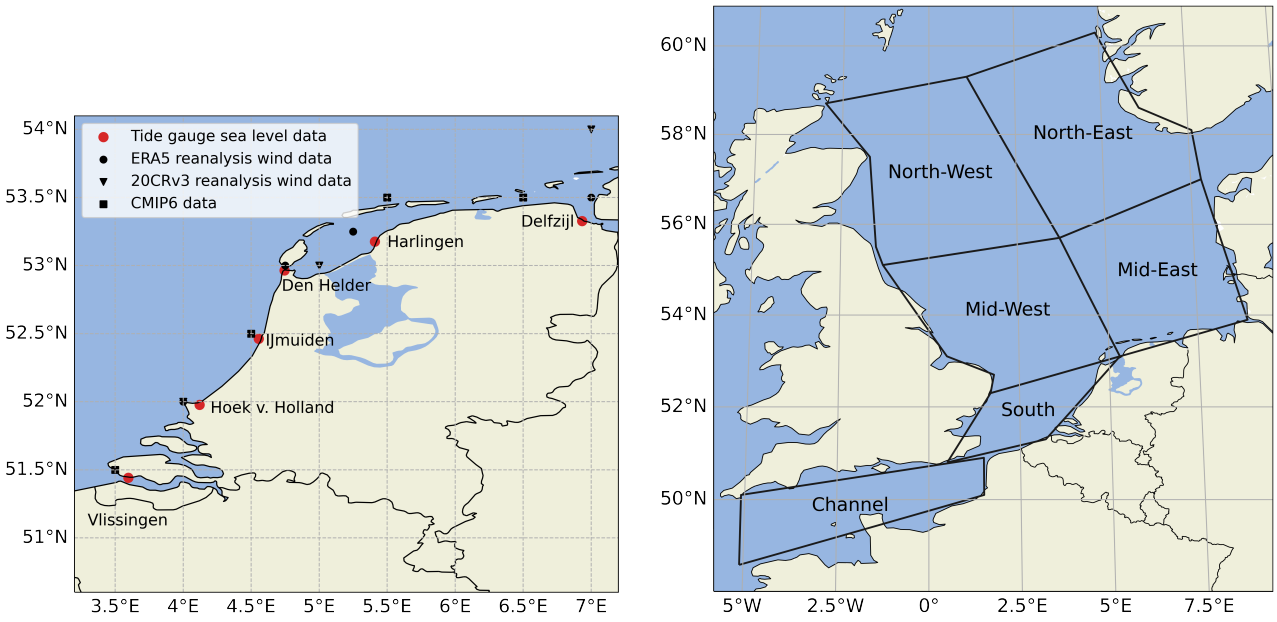

(a) Locations of reanalysis and CMIP6 data used for the NearestPoint regression model.

(b) The 6 regions that are used to take averages of wind data from for the Timmerman regression model.

Figure 4: Locations of which wind data is obtained to use for the NearestPoint and Timmerman regression models.

the average RSLC of the tide gauge stations is regressed with the average zonal and meridional wind forcing of the 6 stations using the same equation. Using equation 6, the RSLC can be reconstructed over the whole available period for the wind data. The wind influence on sea-level changes is reconstructed using the underlined expression in equation 6.

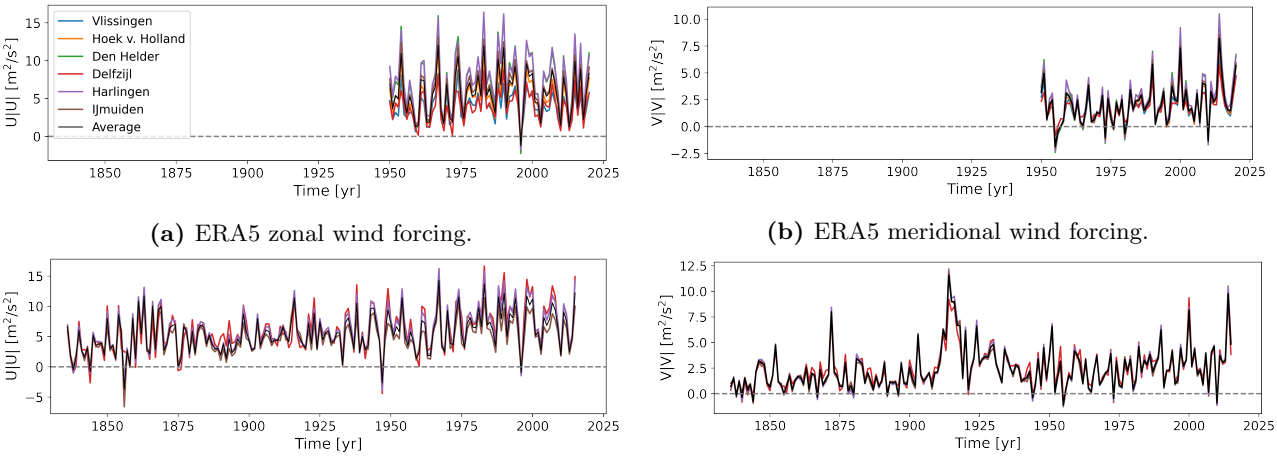

(a) ERA5 zonal wind forcing.

(b) ERA5 meridional wind forcing.

(c) 20CRv3 zonal wind forcing.

(d) 20CRv3 meridional wind forcing.

Figure 5: Wind forcing data used in the NearestPoint regression model. The time series are obtained by selecting wind data nearest to the tide gauge station and above the sea. The locations of which data is retrieved can be found in Fig. 4a.

3.1.3 Timmerman Regression Model

The surge or lowering of water levels along the Dutch coast is not only due to local wind forcing. Therefore, including wind forcing data from a broader region might yield different results. The Timmerman regression model does take that into account by using averages of wind forcing from 6 regions across the North Sea and the English Channel, and these regions are shown in Fig. 4b. This regression model is inspired by the Timmerman surge model that KNMI has long employed to predict surges along the Dutch coast [Timmerman 1975]. Zonal and meridional wind forcing from these Timmerman regions are the explanatory variables in this regression model. For each region, the 10 m zonal and meridional wind speeds are averaged and used to represent wind

forcing by multiplying their values with the absolute values. The resulting time series of wind forcing are shown in Fig. 6. For each tide gauge station and their average, RSLC is reconstructed using the average zonal and meridional wind forcing of the 6 regions. Thus, the Timmerman regression model can be expressed as:

$$\eta(t) = \alpha + \beta_{\mathrm{tr}} \cdot \mathrm{tr}(t) + \sum_{i=1}^{6} \underline{\left[\beta_{u,i} \cdot U_i(t)|U_i(t)| + \beta_{v,i} \cdot V_i(t)|V_i(t)| \right]} + \epsilon(t). \tag{7}$$

In this equation, the summation sign denotes the summation over the six regions of which wind stress averages are obtained. RSLC can be reconstructed for the whole available wind data period using the equation above. Again, the underlined part of equation 7 denotes the wind influence on sea-level change (AC).

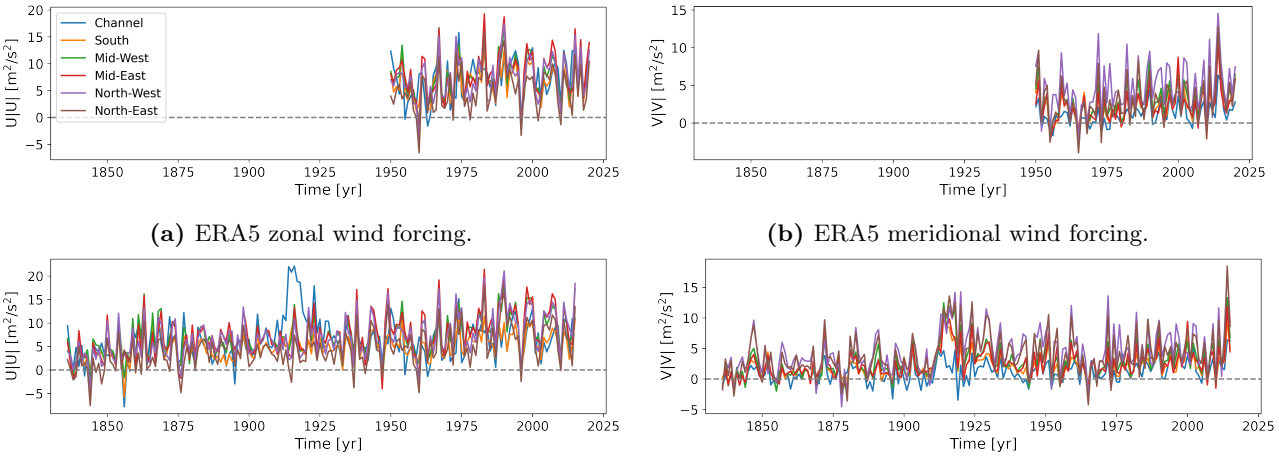

(a) ERA5 zonal wind forcing.

(b) ERA5 meridional wind forcing.

(c) 20CRv3 zonal wind forcing.

(d) 20CRv3 meridional wind forcing.

Figure 6: Wind forcing data used in the Timmerman regression model. The time series are obtained by averaging wind data within the 6 Timmerman regions. These regions are shown in figure 4b.

Since the Timmerman regression model includes many more forcing variables than the other regression models, the chances of overfitting are higher. Therefore, a least absolute shrinkage and selection operator (LASSO) regression model is used for this model rather than a linear regression model. LASSO is a regression analysis where both variable selection and regularisation are applied to encourage a sparse model, with fewer parameters [Tibshirani 1996]. More simply said, the LASSO regression model shrinks some regression coefficients and sets others to zero to avoid taking the same process into account more than once. As the wind forcing of the different regions is expected to show multicollinearity, the LASSO model regularises this by giving penalties, and some forcing variables are excluded from the model. The LASSO model uses an L1 regularisation which minimises the absolute value of the sum of the magnitude of the coefficients. Thus, the algorithm minimises:

$$\sum_{t=0}^{T} \left(\eta(t) - \sum_{i} \left(\beta_{u,i} \cdot U_i(t)|U_i(t)| + \beta_{v,i} \cdot V_i(t)|V_i(t)| \right) \right)^2 + \alpha \sum_{i=1}^{6} |\beta_{u,i} + \beta_{v,i}|. \tag{8}$$

Here, α represents the strength of the L1 regularisation, and T represents the final year of the time series included in the regression. When α is zero, the linear regression model is retained. An automated model is used that is fitted repeatedly using different values for α and selects the best value for α, having the highest explained variance, using cross-validation.

3.1.4 Dangendorf Regression Model

The third regression model we use takes wind influence from an even larger region into account. The Dangendorf regression model uses sea level pressure fields over Scandinavia and South-West Europe, as was done similar in [Dangendorf, Wahl, et al. 2014.] The detrended RSLC of the tide gauge stations and their average is correlated with sea level pressure (SLP) fields over an area extending from 0°N to 90°N and from 90°W to 90°E using the ERA5 and 20CRv3 reanalysis data. These correlations show a robust negative correlation between RSLC and SLP over Scandinavia and a strong positive correlation over the Iberian Peninsula and the Maghreb, as is shown in Fig. 7. These plots show the correlation results over the overlapping period from 1950 to 2015 for both reanalysis data sets. However, the correlation resulting from both data sets shows a similar negative correlation region, the positive correlation region is weaker for the 20CRv3 results. The positive and negative correlation regions are obtained for different periods. Similar as Dangendorf found for the German Bight, the

centres of correlation are a stable phenomenon for the Dutch coast. As stated in [Dangendorf, Wahl, et al. 2014], these correlation patterns reflect zonal wind flow over the North Sea and indicate the dominant influence of zonal wind stress on sea-level variability. [Dangendorf, Wahl, et al. 2014] shows how persistent wind blowing over the North Sea drives a counter-clockwise circulation and piles up water at the southeastern coastlines. In the Dangendorf regression model, the positive and negative correlation areas represent wind stress forcing. The average SLP is obtained over the positive correlation area (20°W-20°E, 25°N-45°N) and the negative correlation area (0°E-40°E, 55°N-75°N). The resulting time series can be found in Fig. 8. RSLC is reconstructed using the average SLP from the positive and negative correlation areas for each tide gauge station and their average. The Dangendorf regression model can thus be expressed as:

$$\eta(t) = \alpha + \beta_{\text{tr}} \cdot \text{tr}(t) + \underline{\beta_n \cdot P_n(t) + \beta_p \cdot P_p(t)} + \epsilon(t). \tag{9}$$

Here, P_n and P_p represent the average sea level pressure over the negative and positive correlation areas.

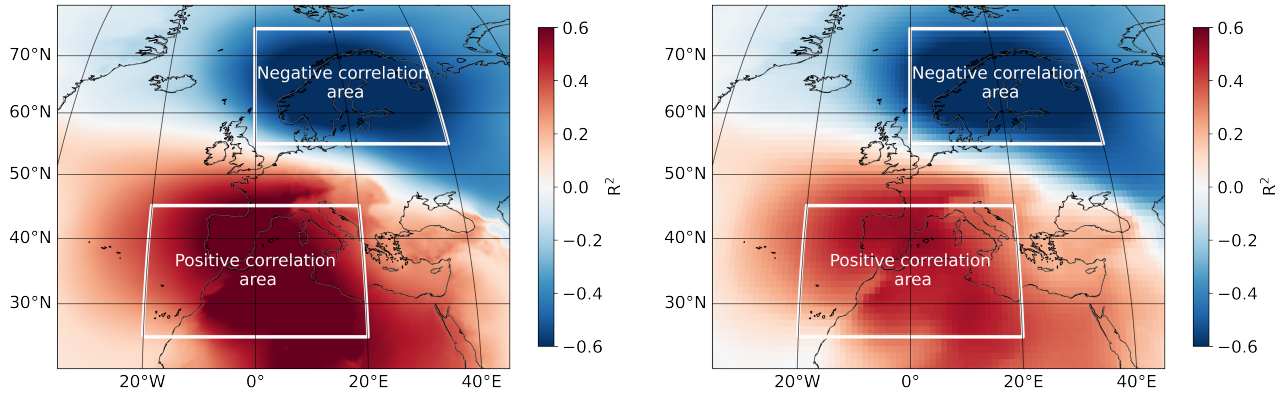

(a) ERA5 reanalysis data. **(b)** 20CRv3 reanalysis data.

Figure 7: Map of the correlation between average sea-level change of the six tide gauges along the Dutch coast and sea level pressure over Europe and the Northern Atlantic region over the period from 1950 till 2015. Also, the regions used to take averages of sea level pressure for the Dangendorf regression model are shown.

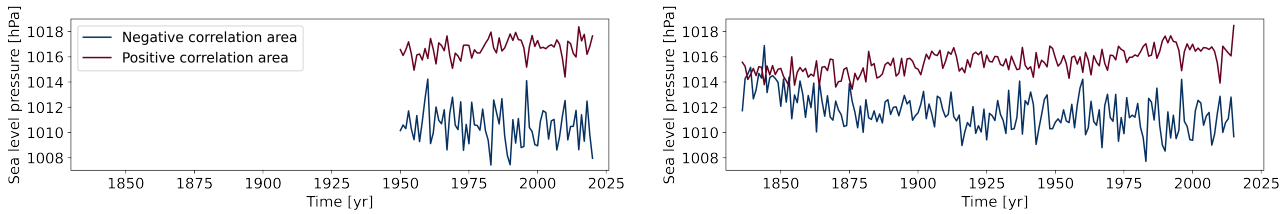

(a) ERA5 reanalysis data. **(b)** 20CRv3 reanalysis data.

Figure 8: Mean sea level pressure averaged over the positive and negative correlation regions as depicted in figure 7.

3.1.5 Analysis of the Regression Results and Model Evaluation

After performing the regression analyses, we can analyse the wind influence on sea-level changes along the Dutch coast over the historical period. Using these time series, we can study the structural change of the wind influence by obtaining linear trends. To study the long-term variability of the wind influence, the time series are smoothed using a Locally Weighted Scatterplot Smoothing (LOWESS) function with a 31-year window. Also, we study the wind-driven variability by obtaining linear trends of the wind influence over periods of 39 years from the whole time series.

There are different metrics to evaluate the performance of regression models. The root mean squared error (RMSE) and R Square (R^2) are studied. RMSE is an absolute measue of how well the model is fitted and is calculated using:

$$RMSE = \sqrt{\frac{1}{N}\sum_{i=1}^{N}(y_i - \hat{y}_i)^2}. \tag{10}$$

In this equation, N is the number of observations, y denotes the dependent variable, which is the RSLC in this study and $\hat{y}$ is the predicted output from the regression model. Therefore, $y_i - \hat{y}_i$ denotes the prediction

error. RMSE explains how much the predicted results deviate from the RSLC and is an excellent metric for comparing different models [Heij et al. 2004]. R^2 is the square of the Correlation Coefficient and is also called the coefficient of determination. It measures the fraction of total variation of the dependent variable that is explained by the model and is calculated using:

$$R^2 = 1 - \frac{\sum_i (y_i - \hat{y}_i)^2}{\sum_i (y_i - \overline{y})^2}. \tag{11}$$

In this equation, again, y is the dependent variable, the RSLC, $\hat{y}$ is the predicted output and $\overline{y}$ is the mean of the RSLC. This means that the numerator is the unexplained variance, and the denominator is the total variance. Thus indeed, R^2 represents the fraction of total variance that is explained by the regression model and has a value between 0 and 1 [Heij et al. 2004].

3.2 The Influence of the Atlantic Multidecadal Variability on Wind-Driven Sea-Level Variability

To identify large-scale drivers of the wind-driven sea-level variability, we study the influence of the AMV using again a linear regression analysis. Yet, in this case, the dependent variable is the wind-driven sea-level variability and we now use a single variable linear regression. Thus, the AMV time series is the only explanatory variable. The used regression model thus reconstruct the wind-driven sea-level variability, or atmospheric contribution to sea-level change (AC), and can be expressed as:

$$AC(t) = \alpha + \beta_{\mathrm{AMV}} \cdot AMV(t - l) + \epsilon(t). \tag{12}$$

Again, α is a constant, β_{AMV} is the regression coefficient, and ϵ is an error term for each moment in time. The underlined expression in equation 12 represents the reconstructed influence of the AMV on the AC. As there might be a time lag in the influence of the AMV and the AC, the regression is performed for shifting the AMV distribution forward in time using different lags (l). Therefore, in equation 12, l represent the lag in years which is varied between 0 and 20 years. This regression analysis is performed using the three different data sets for AMV, HadISSTv2, ERSSTv2 and COBE-SST2, the AC resulting from the ERA5 and 20CRv3 reanalysis and the NearestPoint, Timmerman and Dangendorf regression models. The regression using the ERA5 reanalysis data is performed from 1950 to 2018, and the regression using the 20CRv3 reanalysis data is performed from 1870 to 2015. Since we want to study the influence of the AMV on the multi-decadal variability, we use time series that are detrended and smoothed with a 31 yr window. The resulting time series for the AMV are shown in Fig. 9. After performing the regression, the influence of the AMV can be reconstructed over the period from 1870 to 2018. To analyse the difference in the results between the two reanalysis data sets, the regression is also performed over the overlapping period from 1950 to 2015. R^2 resulting from the regression analyses is studied to understand the variance explained by the AMV. The sign of the regression coefficients are examined to see whether there is a direct or inverse relationship between the AMV and wind-driven sea-level variability.

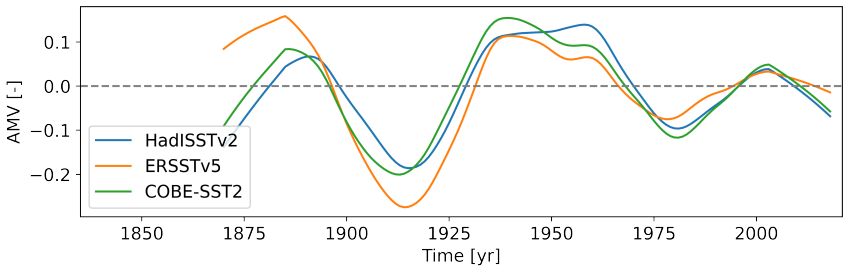

Figure 9: Plot of the detrended and smoothed time series of the Atlantic Multidecadal Variability for the HadISSTv2, ERSSTv5 and COBE-SST2 data sets. The time series are smoothed using a 31-year LOWESS function.

3.3 The Influence of Sea Surface Temperature on Wind-Driven Sea-Level Variability

The AMV is a multi-decadal mode of variability that is constructed from sea surface temperature data over a region in the Northern Atlantic ranging from 0°N to 60°N and from 80°W to 0°E. However, some subregions might contribute more or less to the multidecadal variability of wind influence along the Dutch coast. Therefore, the influence of local sea surface temperature (SST) in the North Atlantic region on the AC is investigated. A similar approach is used as described in the previous section. For each SST data point located between 0°N and 90°N and 100°W and 10°E, the influence on the AC is analysed using linear regression. Again, the SST

and AC time series are detrended, and a LOWESS function with a 31-year window is applied. A simple linear regression is performed using the sea surface temperature as a forcing variable, and the reconstructed AC can thus be expressed as:

$$AC(t) = \alpha + \beta_{\mathrm{SST}} \cdot SST(t) + \epsilon(t). \tag{13}$$

As before, α is a constant, β_{SST} is the regression coefficient and ϵ is a residual for each moment in time. Unlike the regression analysis with the AMV, the regression is now executed without a lag. The regression analysis is performed with the SST ERSSTv5 data and SKT 20CRv3 data and the atmospheric contribution resulting from ERA5 and 20CRv3 data using the NearestPoint, Timmerman and Dangendorf regression models. Again, the coefficients of determination are studied to understand the explained variance and the sign of the regression coefficients are examined to see if the relationship is direct or inverse.

3.4 The Wind Influence on Sea-Level Change over the Historical Period using Climate Models

After we studied the wind influence on sea-level change along the Dutch coast using observations and reanalysis data and three regression models. We perform the same analysis over the historical period using CMIP6 climate model data. As the dependent variable, we use the annual mean dynamic sea level, which of which we obtain the nearest neighbour data points for each tide gauge station. These locations are shown in Fig. 4a. The dynamic sea level data does not have to be corrected for the nodal cycle and the IBE. For the NearestPoint regression model, we obtain wind speed from the same locations as the dynamic sea level data. For the Timmerman and Dangendorf models, we average data from the climate models over the same regions as used for the observational data. Otherwise, the method for the three regression models is the same as described in Section 3.1. However, the regression analysis is only performed for the average sea-level change along the Dutch coast and not for the individual stations but in this case using all 28 climate models as given in Tab. 6.

After performing the regression, two methods are used to validate how well the climate models reproduce the wind influence on sea-level change we found using observations. First, a multitaper spectral analysis is performed [Thomson 1982]. Similar to the well known Fourier analysis, the multitaper method is a technique to estimate the power spectrum. However, compared to the Fourier analysis, there is more temporal precision for high-end and low-end frequencies making this a valuable method to use for our time series with substantial interannual variability and a multi-decadal variation Yiou, Baert, and Loutre 1996; Babadi and Brown 2014. The multi-taper analysis is performed for the 20CRv3 wind influence on sea-level change and the climate model data from 1850 to 2015 for the results of the three regression models. Before performing the spectral analysis, we detrend the time series. As a next step, the power spectral density is used to calculate the variance of the entire signal (total variance) and the variance of the signal having a period between 30 and 80 years (partial variance) as this is the time scale of results that is most relevant for this study. Then, for the results of each regression model, the climate model results are compared to the observational results. The results of the total variance are plotted against the partial variance, and the euclidean distance between the observational result and each climate model data result is calculated. As a final step, the average Euclidean distance of the three regression models is obtained, and the climate models are selected as best performing when their average euclidean distance is smallest.

Thereafter, also a Kolmogorov-Smirnov-test (KS-test) is performed, as was similarly done in Dangendorf, Wahl, et al. 2014. The KS-test is a nonparametric test for the equality of continuous, one-dimensional probability distributions. It examines whether two samples are drawn from the same statistical population by measuring the distance between the empirical distribution of both samples:

$$D_{KS} = \max_{x} |F_X(x) - F_Y(x)|. \tag{14}$$

In this study, the distance is calculated between wind influence resulting from the regression analyses with the 20CRv3 reanalysis and climate model data from 1850 to 2014. Climate models perform best when the distance resulting from the KS-test is most minor, and the results are statistically significant. Again, we use detrended time series in the KS-test. The best performing climate models are selected as the 50% that perform best for both tests for further analysis. After that, the linear trends of these climate models and the resulting time series of the wind influence on sea-level change are compared to the observational results. As climate models are only a simulation of the actual physical system and are restricted to understanding physical processes, the models can not be expected to perfectly reproduce the wind influence as found using the observational data.

3.5 Projecting the Wind Influence on Sea-Level Change into the 21st Century

When the wind influence on sea-level change has been analysed over the past period, and it is validated which climate models can reproduce this wind influence, the output from these climate models over the historical period can be used to make projections of the wind influence on sea-level change for the 21st century.

As described in Section 3.4, the regression analysis with the three regression models is also executed using CMIP6 historical model data. Thereby for each climate and regression model, regression coefficients are obtained that we use for the projections. In the NearestPoint regression model, for each climate model and each scenario again, zonal and meridional wind speed data is obtained from the exact locations described in the previous section. The average zonal and meridional wind speed of the 6 locations is obtained and used together with the regression coefficients obtained over the historical period to obtain projections for the 21st century. The wind influence, or atmospheric contribution (AC) is thus obtained using:

$$AC(t) = \beta_u \cdot U(t)|U(t)| + \beta_v \cdot V(t)|V(t)| \tag{15}$$

In the Timmerman regression model for each climate model and each scenario, zonal and meridional wind speed averages of each Timmerman region are obtained. These averages are used to obtain projections of the atmospheric contribution to sea-level change using:

$$AC(t) = \sum_{i=1}^{6} \left[\beta_{u,i} \cdot U(t)|U(t)| + \beta_{v,i} \cdot V(t)|V(t)| \right] \tag{16}$$

where again the coefficients $\beta_{u,i}$ and $\beta_{v,i}$ result from the regression over the historical period.
In the Dangendorf regression model, sea level pressure data is averaged over the regions of positive and negative correlation for each climate model and each scenario. Again, these averages are used to obtain projections of atmospheric contribution to sea-level change using:

$$AC(t) = \beta_n \cdot P_n(t) + \beta_p \cdot P_p(t). \tag{17}$$

Again, the regression coefficient results from the regression over the historical period.

4 Results

4.1 The Wind Influence on Sea-Level Change over the Historical Period using Observations

First, the results are shown to answer the most critical question: What was the wind influence on sea-level changes over the past period? Before analysing the results to answer this question, we compare the performance using the different regression models and reanalysis data sets. The RMSE and R^2 results from the regression analysis are shown in Tab. 1. The RMSE values of the different regression analyses lie close together. These values suggest that the Timmerman model performs slightly better than the other two. We do not only calculate R^2 for the whole model (R^2_{total}) but also for only the part of the model that reconstructs the wind influence (R^2_{wind}). The values of R^2_{total} are much higher than the values of R^2_{wind} which is due to the fact that the trend is included in the regression models and explains the most considerable fraction of the total variance of the RSLC. The values of R^2_{wind} show that using the 20CRv3 data and the Timmerman regression model is best at reconstructing the wind influence. Using the ERA5 data, both the Timmerman and Dangendorf regression models better reconstruct the wind influence than the NearestPoint regression model. The Dangendorf regression model's R^2 values are higher for the ERA5 data. This might be caused by the fact that the reanalysis data of mean sea level pressure before 1950 is less good. Also, Figure 7 shows that the positive correlation area is weaker for the 20CRv3 data than the ERA5 data. This indicates that using the mean sea level pressure data as a proxy for wind forcing works less well for the 20CRv3 data than the ERA5 data.

Table 1: Results from the regression with the three regression models for observational and reanalysis data for the average RSLC. The regression is performed using ERA5 data from 1950 to 2020 and 20CRv3 data from 1836 to 2015.

	NearestPoint		Dangendorf		Timmerman	
Metric	ERA5	20CRv3	ERA5	20CRv3	ERA5	20CRv3
RMSE [cm]	2.1	2.1	2.0	2.2	1.9	1.9
R^2_{total} [%]	86	93	87	92	89	94
R^2_{wind} [%]	19	29	36	29	33	40

The regression analyses are performed for each tide gauge station and their average. In this section, only the results for their average are shown. More detailed results for the individual stations can be found in the Appendix Section A. There are no substantial differences between the results of the average of the stations and the individual stations. The regression coefficients resulting from the regression analysis are shown in Tab. 2. These regression coefficients and the atmospheric reanalysis data are used to reconstruct the wind influence on sea-level changes. Figure 10 shows for the different regression models the contributions to the wind influence. For the NearestPoint and Timmerman model, the zonal and meridional contributions are shown, and for the Dangendorf model, the contribution of the negative and positive correlation areas. These results show that the zonal contribution plays a dominant role in explaining the sea-level variability. For the Dangendorf model, the contribution of both mean sea level pressure time series is quite similar. This would also be expected as the gradient between the pressure differences drives the wind forcing over the North sea.

Table 2: Results from the regression with the three regression models for observational and reanalysis data for the average RSLC.

Regression coefficients	NearestPoint ERA5	NearestPoint 20CRv3		Dangendorf ERA5	Dangendorf 20CRv3		Timmerman ERA5	Timmerman 20CRv3
α	7.38	-4.09	α	7.38	-4.59	α	7.38	-3.99
β_{tr}	4.54	9.52	β_{tr}	4.08	9.54	β_{tr}	4.16	9.09
β_{u^2}	2.32	2.13	β_n	-1.44	-1.53	$\beta_{u^2}^{\text{Channel}}$	0.43	0.12
β_{v^2}	-0.29	-0.13	β_p	1.18	1.03	$\beta_{v^2}^{\text{Channel}}$	0.20	1.07
						$\beta_{u^2}^{\text{South}}$	0	0.43
						$\beta_{v^2}^{\text{South}}$	0	-0.31
						$\beta_{u^2}^{\text{Mid-West}}$	0	0.26
						$\beta_{v^2}^{\text{Mid-West}}$	0	0
						$\beta_{u^2}^{\text{Mid-East}}$	2.09	0.74
						$\beta_{v^2}^{\text{Mid-East}}$	-0.04	0
						$\beta_{u^2}^{\text{North-West}}$	0	0.81
						$\beta_{v^2}^{\text{North-West}}$	-0.71	-0.78
						$\beta_{v^2}^{\text{North-East}}$	-0.07	0
						$\beta_{v^2}^{\text{North-East}}$	0	0.13

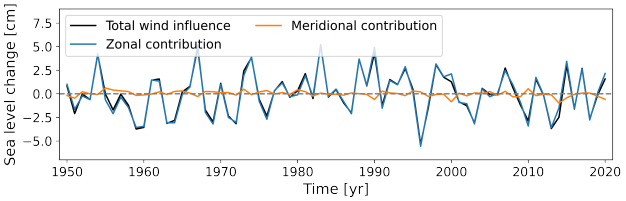

(a) NearestPoint regression model and ERA5 reanalysis data.

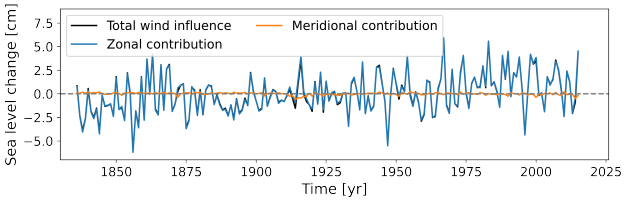

(b) NearestPoint regression model and 20CRv3 reanalysis data.

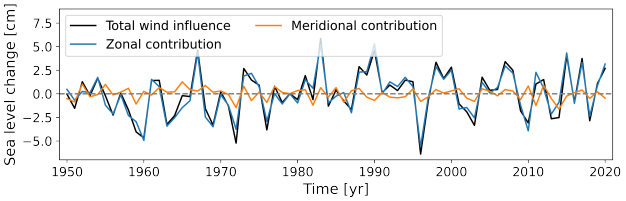

(c) Timmerman regression model and ERA5 reanalysis data.

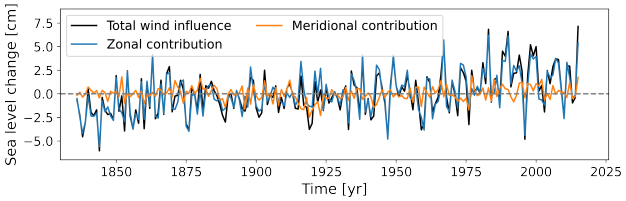

(d) Timmerman regression model and 20CRv3 reanalysis data.

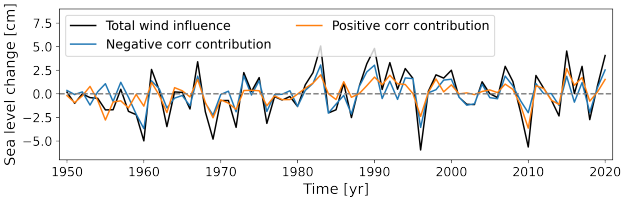

(e) Dangendorf regression model and ERA5 reanalysis data.

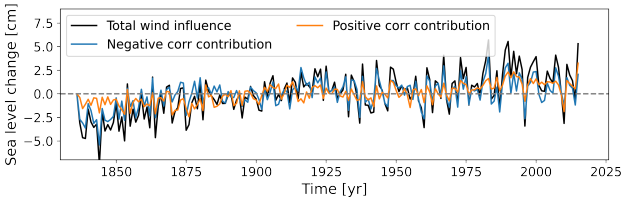

(f) Dangendorf regression model and 20CRv3 reanalysis data.

Figure 10: Time series of the zonal and meridional wind contribution to sea-level change resulting from the NearestPoint and Timmerman regression model and the contribution of the negative and positive correlation areas to sea-level change from the Dangendorf regression model.

Table 3: Linear trends of the atmospheric contribution to sea-level changes resulting from the regression analyses with observational sea level data and atmospherical reanalysis data. The time series whereof the trends are calculated are shown in Figs. 11a and 11b. The trends have units mm/yr and an error of one standard deviation (σ).

Period	NearestPoint ERA5	NearestPoint 20CRv3	Dangendorf ERA5	Dangendorf 20CRv3	Timmerman ERA5	Timmerman 20CRv3	RSLC
1950 - 2020	0.04 ± 0.13	-	0.27 ± 0.14	-	0.21 ± 0.14	-	2.1 ± 0.2
1836 - 2015	-	0.14 ± 0.03	-	0.27 ± 0.03	-	0.20 ± 0.03	-

For each regression analysis the wind influence on sea-level change is obtained and shown in Figs. 11a and 11b. These plots show that the wind influence varies around zero, raising and lowering sea level with maximum values between 5.1 and 7.4 cm and a standard deviation between 2.1 and 2.5 cm for the results of the different analyses. We used these time series to obtain linear trends to examine the structural change of the wind influence on sea-level changes. The resulting linear trends are shown in Tab. 3. The results range from 0.04 ± 0.13 mm/yr for the NearestPoint model using ERA5 data to 0.27 ± 0.14 mm/yr for the Dangendorf model using ERA5 data. The standard deviations are more minor for the results using the 20CRv3 data, which indicate a linear trend between 0.1 and 0.3 mm/yr where the result with the highest R^2_{wind}, from the Timmerman, lies precisely in the middle with 0.20 ± 0.03 mm/yr. These values suggest that the fraction of the total long-term structural change in sea level due to wind influence lies between 5% and 15%.

The long-term wind-driven sea-level variability becomes apparent when the atmospheric contribution to sea-level change is smoothed. Therefore, a LOWESS function with a 31-year window is applied. This result is shown in Fig. 11c. This plot shows the importance of the structural change of the wind influence over centuries, but over shorter periods also, a robust multi-decadal mode of variability is essential. When the atmospheric contribution is detrended before applying the smoothing function, as is shown in Fig. 11d, it can be seen that this multi-decadal wind-driven sea-level variability has an amplitude of 1 cm and a period of 40 to 60 years. From 1950 to 2010, the wind-driven multi-decadal sea-level variability is similar for the results from different regression models and reanalysis products. However, before 1950 the results from the analyses with different regression models are less similar. Between about 1960 and 1990, the wind influence increased and decreased again between 1990 and 2005. The results obtained using the ERA5 reanalysis, which extends until 2020, show that the wind influence has stabilised over the last decade. Fig. 11e shows the evolution of the linear trends obtained over periods of 39 years. The multidecadal mode of variability is also apparent in these results. The linear trends vary between plus 1 mm/yr and minus 0.5mm/yr and for recent decades, the wind dropped sea level by about 0.5 mm/yr. These linear trends over 39 years show that the wind influence on sea-level change started decreasing since the late 1960s. Fig. 11f shows the evolution of the linear trends obtained over periods of 19 years. Also, the results show the multidecadal variability seen in the wind-driven sea-level variability. Calculated over shorter periods, the linear trend reaches above 1.0 mm/yr and below -1.0 mm/yr. These plots also show that the trend of the wind influence decreased since about 1970 but started increasing again around 1990 and has been near zero over the last decade.

We study the impact of these changes of the wind influence by correcting the RSLC averaged over the 6 tide gauges along the Dutch coast for the wind influence as shown in Fig. 11a and 11b. Both the RSLC and the corrected RSLC are smoothed with a 31 yr window and shown in Fig. 12. These plots show that an acceleration of sea-level rise can be observed after removing the wind effect. The best results of the wind influence for the last decade are obtained using ERA5 data, which extends till 2020. Fig. 11d already showed that since 2005 the wind effect stabilized and slightly increased again. In Fig. 12a, it can be seen that indeed for the last 10 or 15 years the trend of the wind effect was zero.

If the wind-driven variability continues its past behaviour as shown in Fig. 11c, for coming decades, the wind influence will increase again and thus raise sea levels. In that case, an acceleration of sea-level rise might also become apparent in the non-corrected tide gauge sea level observations.

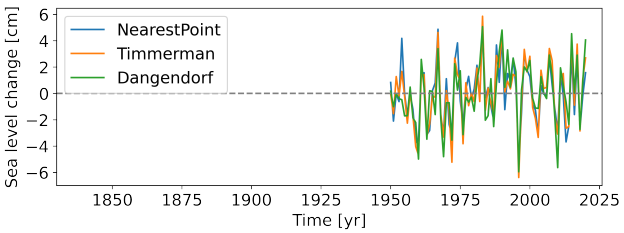

(a) Annual time series of atmospheric contribution to sea-level change using ERA5.

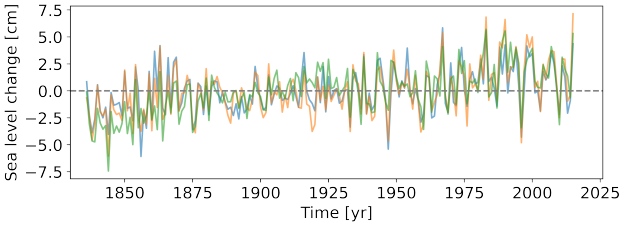

(b) Annual time series of atmospheric contribution to sea-level change using 20CRv3.

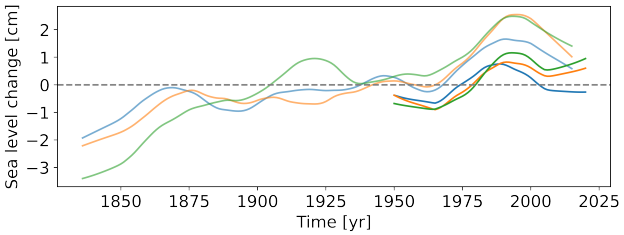

(c) Annual smoothed time series using LOWESS with a 31-year window applied.

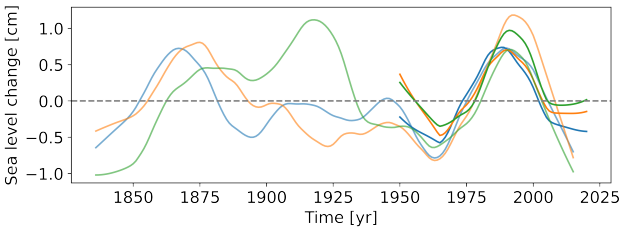

(d) Annual detrended and smoothed time series using LOWESS with a 31-year window applied.

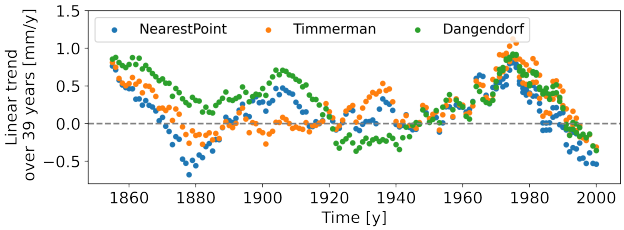

(e) Linear trends calculated over periods of 39 years. The resulting trend is plotted at the centre of that period.

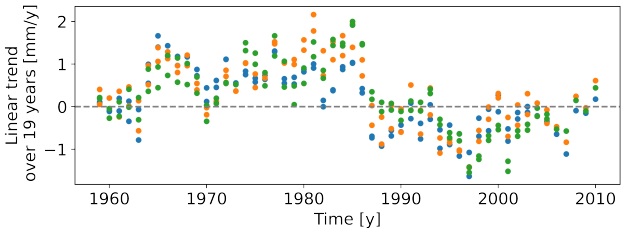

(f) Linear trends calculated over periods of 19 years. The resulting trend is plotted at the centre of that period.

Figure 11: Annual time series of the atmospheric contribution to sea-level change resulting from the regression with observational sea level data and atmospherical ERA5 and 20CRv3 reanalysis data using the NearestPoint, Timmerman and Dangendorf regression models as well as a plot of the linear trends of the atmospheric contribution calculated over periods of 39 years. The bold lines are ERA5 and the transparent lines 20CRv3.

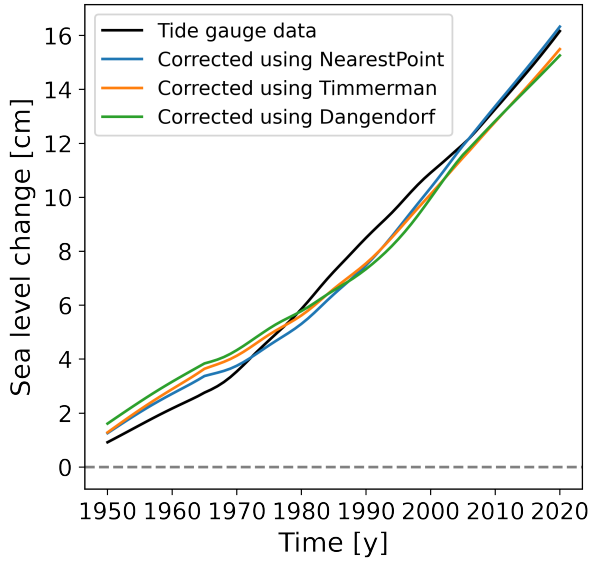

(a) ERA5 reanalysis data.

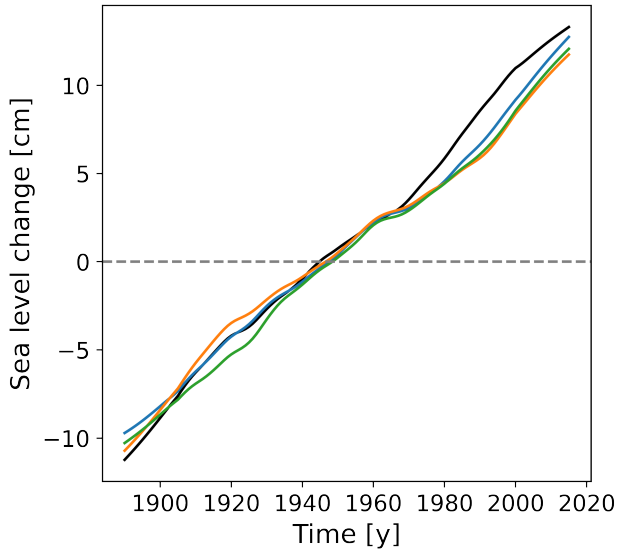

(b) 20CRv3 reanalysis data.

Figure 12: Time series of the sea level measurements averaged over six stations along the Dutch coast smoothed with a 31 yr window and the same time series corrected for the wind influence resulting from the analysis with the three regression models and ERA5 and 20CRv3 reanalysis data

4.2 The Influence of the Atlantic Multidecadal Variability on Wind-Driven Sea-Level Variability

In this section, we show the results of the regression analyses between the detrended and smoothed AMV time series and the multi-decadal wind-driven sea-level variability as shown in Fig. 11d. We study the influence of the AMV to answer the question whether we can identify large-scale drivers of the multi-decadal sea-level variability. The analysis is performed over the overlapping period between the used atmospheric reanalysis product and the AMV data. For the ERA5 reanalysis data, this is from 1950 to 2018, and for the 20CRv3 data from 1870 to 2015. The resulting R^2 values and regression coefficients are shown in respectively Fig. 13a and 13b.

The plots in Fig. 13a show that for all results, the explained variances are highest for a lag between 5 and 10 yr. For these lags, using the ERA5 reanalysis data, for all three regression models, the explained variance reaches values between 50% and 78%. For the 20CRv3 reanalysis results, the results for the different regression models are not consistent. Where the explained variance for the NearestPoint and Timmerman models is only between 0% and 26% at largest, the results for the Dangendorf model are between 35% and 68%. Some of our results do thus indicate that the AMV plays a role as a driver of the multi-decadal sea-level variability. The difference in the results of the regression analyses we find for using the ERA5 or 20CRv3 reanalysis is caused by the different periods used for the study. When the regression analysis is performed for the overlapping period from 1950 to 2015 using the different reanalysis data sets yields similar results as is shown in appendix Section B. Fig. 13b shows that all regression coefficients are negative for most different data products an inverse relationship between the AMV and wind-driven sea-level variability is found. This implies that when AMV values increase, this leads to a sea level drop along the Dutch coast.

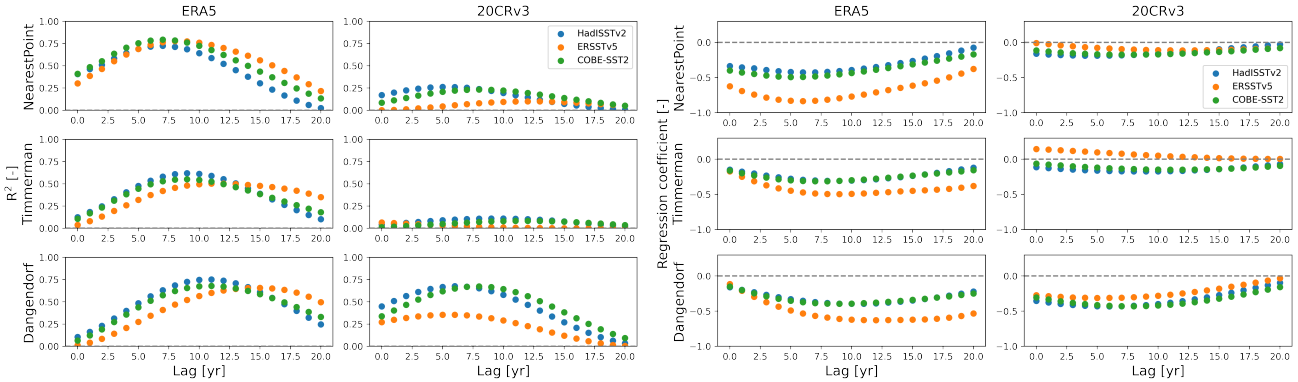

(a) R^2 results of the regression. **(b)** Regression coefficient (β_{AMV}) results of the regression.

Figure 13: Plots of R^2 and the regression coefficient (β_{AMV}) for the regression between the detrended and smoothed AMV and wind-driven sea-level variability. Both R^2 and β_{AMV} are plotted against the time lag (l).

The AMV influence on sea-level changes resulting from the regression analysis with the wind-driven sea-level variability are shown in Figs. 14 and 15. These plots show the results obtained from the regression with respectively the ERA5 or 20CRv3 wind-driven sea-level variability as the dependent variable. For the ERA5 results, the regression is performed from 1950 to 2018. Over this period, the wind-driven sea-level variability shows one peak, making it easier to obtain a good fit for the AMV data. Especially for a lag of 5 or 10 years the AMV data is fitted well. However, for some results these fits show that before 1950 the AMV influence on wind-driven sea variability has a larger amplitude than 1 cm. This would imply that the AMV influence on the wind-driven sea-level variability would be larger than the amplitude of the wind-driven sea-level variability we found, which is intriguing. This might indicate that the period used for the regression with the ERA5 wind-driven sea-level variability is too short since it only includes one period of the multi-decadal variability. Using the 20CRv3 results, the regression is performed from 1870 to 2015 and thus includes more periods of the multi-decadal variability. However, before 1950 the different regression models match less. For the regression using 20CRv3 wind-driven sea-level variability, the R^2 values are highest for the Dangendorf regression model. The resulting time series, shown in Fig. 15, also show that the AMV is fitted best for the Dangendorf regression model. The link between the AMV and the wind-driven sea-level variability does not look convincing for the NearestPoint and Timmerman models, which agree with the low values for R^2. Nevertheless, the link between the AMV and the multi-decadal sea-level variability does look convincing for the results of the Dangendorf regression model for lags of 0, 5 and 10 years.

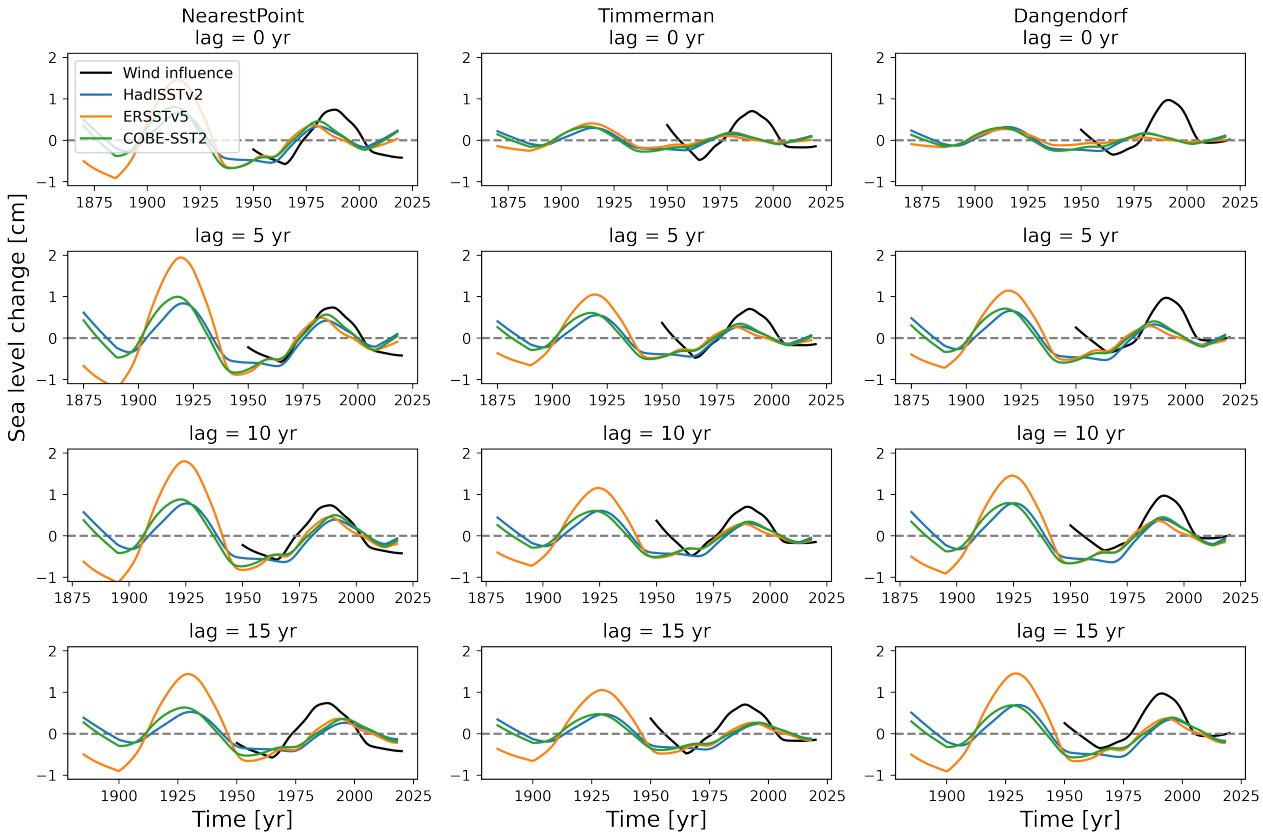

Figure 14: Plot of the dependent variable, ERA5 wind-driven sea-level variability, and the AMV influence on sea-level change resulting from the regression analysis using lags of 0, 5, 10 and 15 yr.

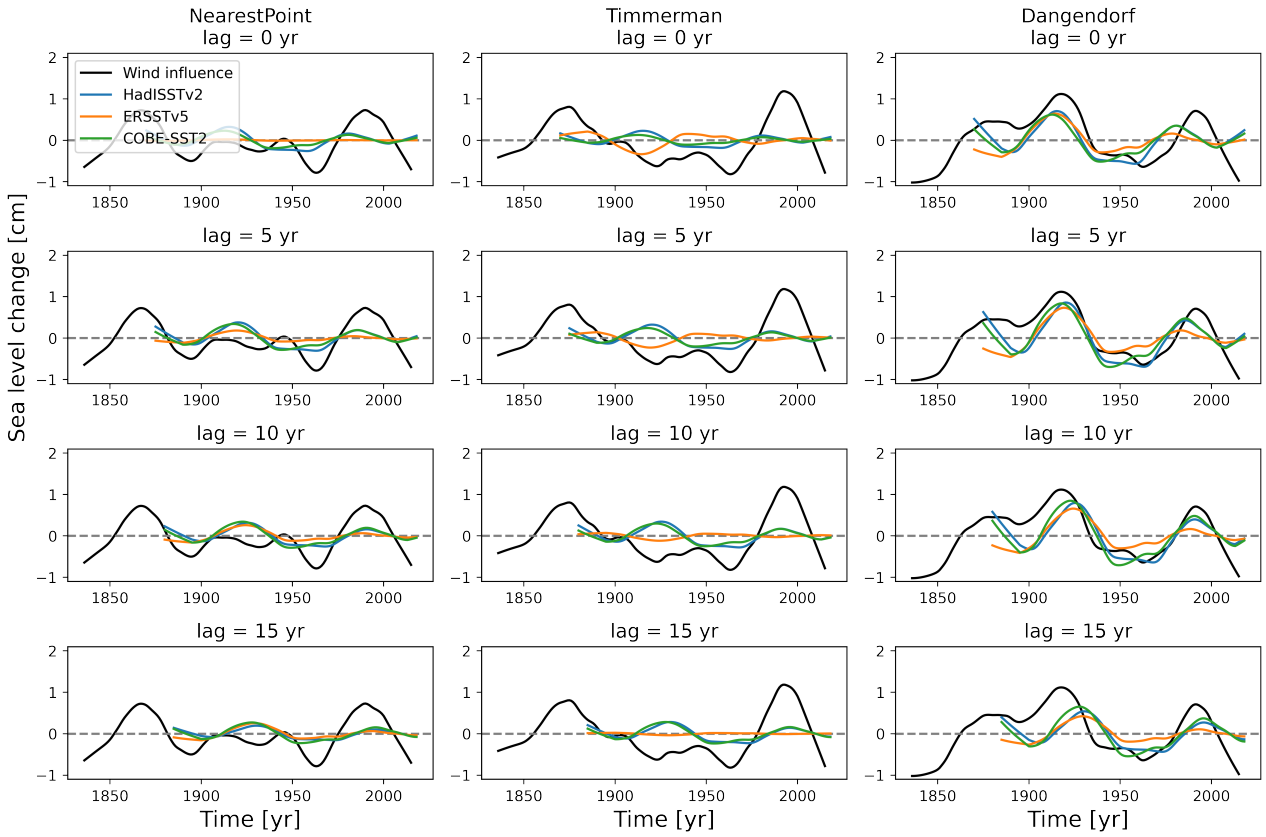

Figure 15: Plot of the dependent variable, 20CRv3 wind-driven sea-level variability, and the AMV influence on sea-level change resulting from the regression analysis using lags of 0, 5, 10 and 15 yr.

4.3 The Influence of Sea Surface Temperature on Wind-Driven Sea-Level Variability

The previous section showed that we could link the AMV to the multi-decadal wind-driven sea-level variability. The AMV is a multi-decadal mode of variability obtained from sea surface temperatures in the North Atlantic Ocean. To better understand the link between the AMV and the wind-driven sea-level variability in this section, we show the results of the influence of SST in the North Atlantic Ocean on the wind-driven sea-level variability. For some regions in the North Atlantic Ocean the link between SST and the wind-driven sea-level variability along the Dutch coast might be stronger than for others. Therefore, we again perform a regression analysis with the wind-driven sea-level variability as the dependent variable. However, now local time series of SST are the explanatory variable and no lag is taken into account. In this section we only show the result of the analysis with ERSSTv5 SST data as they are similar to the results using surface skin temperature (SKT) data, whereof the results are shown in appendix Section C.

Maps showing the resulting R^2 values and regression coefficients of the analysis are shown in Fig. 16. From these maps some regions can be identified with higher values for R^2 (Figs. 16a and 16b), especially for the analysis with ERA5 data and the NearestPoint regression model and 20CRv3 data and the Dangendorf regression model. These are the same regression analyses with higher R^2 values for the regression with the AMV data for a lag of 0 years as is shown in Fig. 13a. For the analysis using ERA5 data and the NearestPoint regression model, explained variances up to 70% are found along the Eastern American coast, from the Equator to the latitude of New York, as well as around southern Greenland and Iceland. For the analysis using 20CRv3 data and the Dangendorf regression model, explained variances up to 60% are also found along the Eastern American coast extending even more towards the middle of the ocean. For this analysis, explained variances up to 40% are found for regions along the coast around the North Atlantic gyre. However, the explained variances around Greenland and Iceland are much lower. Similar to the results of the analysis with the AMV, the regression coefficients are negative for all these regions. For the analysis using 20CRv3 data and the Timmerman regression model, high R^2 values can be found above 60%, in the southeast part of the North Atlantic Ocean. However, these high explained variances are connected to positive regression coefficients.

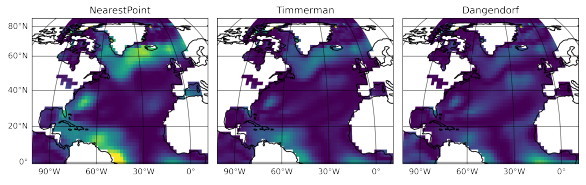

(a) Coefficients of determination resulting from the regression with ERA5 reanalysis data over the period from 1950 to 2018.

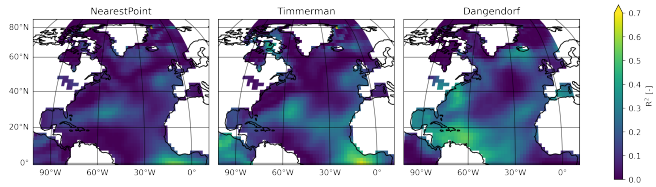

(b) Coefficients of determination resulting from the regression with 20CRv3 reanalysis data over the period from 1870 to 2015.

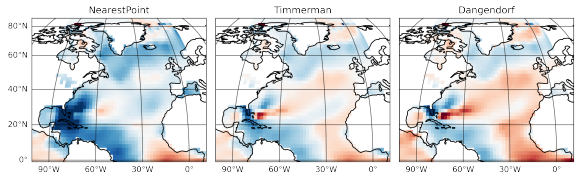

(c) Regression coefficient resulting from the regression with ERA5 reanalysis data over the period from 1950 to 2018.

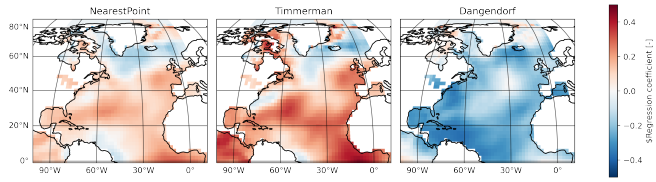

(d) Regression coefficient resulting from the regression with 20CRv3 reanalysis data over the period from 1870 to 2015.

Figure 16: Results of the regression between SST and atmospheric contribution to sea-level change using ERSSTv5.

4.4 The Wind Influence on Sea-Level Change over the Historical Period using Climate Models

In previous sections, we showed the results of the wind influence on sea-level change over the historical period using observational data. This section will show the same analysis results using climate model data. The 50% of models that are selected as best performing after applying the multi-taper spectral analysis and KS-test are shown in bold in Tab. 6. The wind influence on sea-level change for these best models, smoothed with a 31 yr window, is shown in Fig. 17. It can be seen that indeed some models also show a multi-decadal mode of variability with an amplitude of 1 cm and have periods ranging between 20 and 50 years. What stands out in the results of the climate models is that the wind influence on sea-level change resulting from the three different regression models agrees very well. The difference in the results between the different regression models was much larger for the observational analysis.

Again, we also calculate the linear trends of the non-smoothed wind influence on sea-level change, which are given in Tab. 4. These results show that the linear trends resulting from the analysis with climate models are much smaller than the trends from the study with observations and most are not statistically significant. Climate models with trends closest to the observations are CanESM5, CMCC-CM2-SR5 and MPI-ESM1-2-HR. Their trends lie between 0.05 and 0.10 mm/yr.

Figs. 18 and 19 show the wind influence on sea-level change resulting from both the climate model and observational (20CRv3) analysis to conclude which climate models can be used for the projections of the 21st century. While none of the climate models perfectly reproduce the wind influence found in the observational analysis, which can also not be expected, the model that best looks like the observational results is CAMS-CSM1-0. Other models of which the wind influence is most similar to the observational results are ACCESS-ESM1-5, CanESM5-CanOE, CNRM-CM6-1, GFDL-ESM4 and EC-Earth3-Veg-LR. These models are used for the projections.

Table 4: Linear trends of the wind influence on sea-level change resulting from the regression analyses with climate model data from 1850 to 2014. The trends have units mm/yr and are reported with an error of one standard deviation (σ). The bold names have trends closest to the observations.

Model	NearestPoint	Timmerman	Dangendorf
ACCESS-CM2	-0.02 ± 0.04	-0.01 ± 0.04	-0.02 ± 0.03
ACCESS-ESM1-5	-0.01 ± 0.03	-0.02 ± 0.05	-0.01 ± 0.03
BCC-CSM2-MR	-0.01 ± 0.02	0.00 ± 0.02	0.02 ± 0.02
CAMS-CSM1-0	0.02 ± 0.03	0.01 ± 0.03	0.02 ± 0.03
CanESM5	0.05 ± 0.03	0.05 ± 0.03	0.10 ± 0.03
CanESM5-CanOE	0.03 ± 0.03	0.03 ± 0.03	0.06 ± 0.03
CMCC-CM2-SR5	0.05 ± 0.03	0.08 ± 0.03	0.08 ± 0.03
CMCC-ESM2	-0.02 ± 0.02	-0.02 ± 0.02	-0.06 ± 0.03
CNRM-CM6-1	0.03 ± 0.04	0.03 ± 0.04	0.03 ± 0.04
EC-Earth3-Veg-LR	-0.02 ± 0.04	-0.02 ± 0.04	-0.04 ± 0.03
GFDL-ESM4	-0.04 ± 0.03	-0.02 ± 0.04	0.04 ± 0.03
MIROC-ES2L	0.00 ± 0.03	-0.02 ± 0.02	-0.04 ± 0.02
MPI-ESM1-2-HR	0.06 ± 0.05	0.05 ± 0.04	0.08 ± 0.04
NESM3	0.08 ± 0.04	0.08 ± 0.04	0.03 ± 0.03
20CRv3	0.15 ± 0.14	0.28 ± 0.15	0.26 ± 0.13

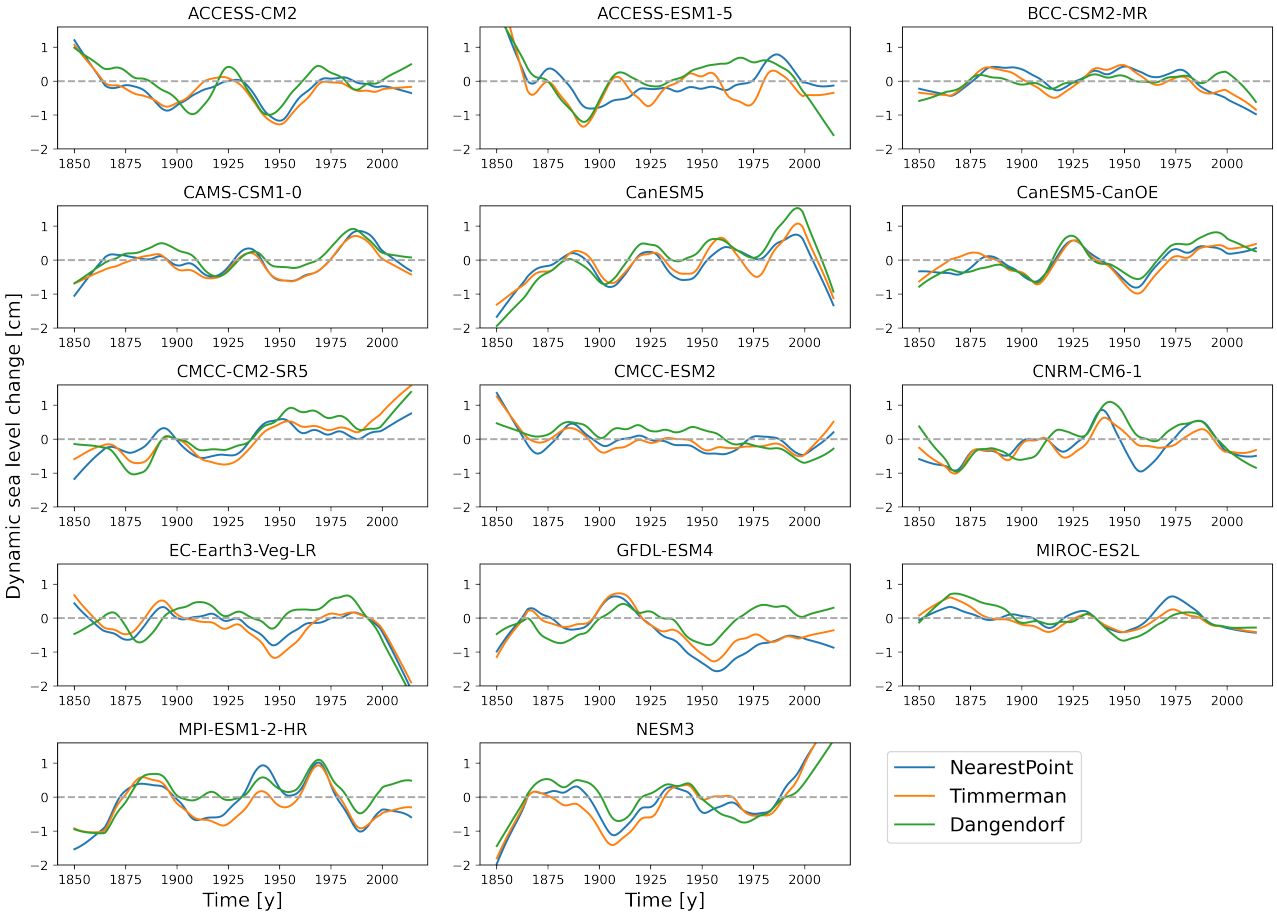

Figure 17: Time series of the wind influence on sea-level change resulting from the regression analyses using climate model data. The time series are shown for the 50% of the climate models that reconstruct the wind influence best compared to the 20CRv3 results.

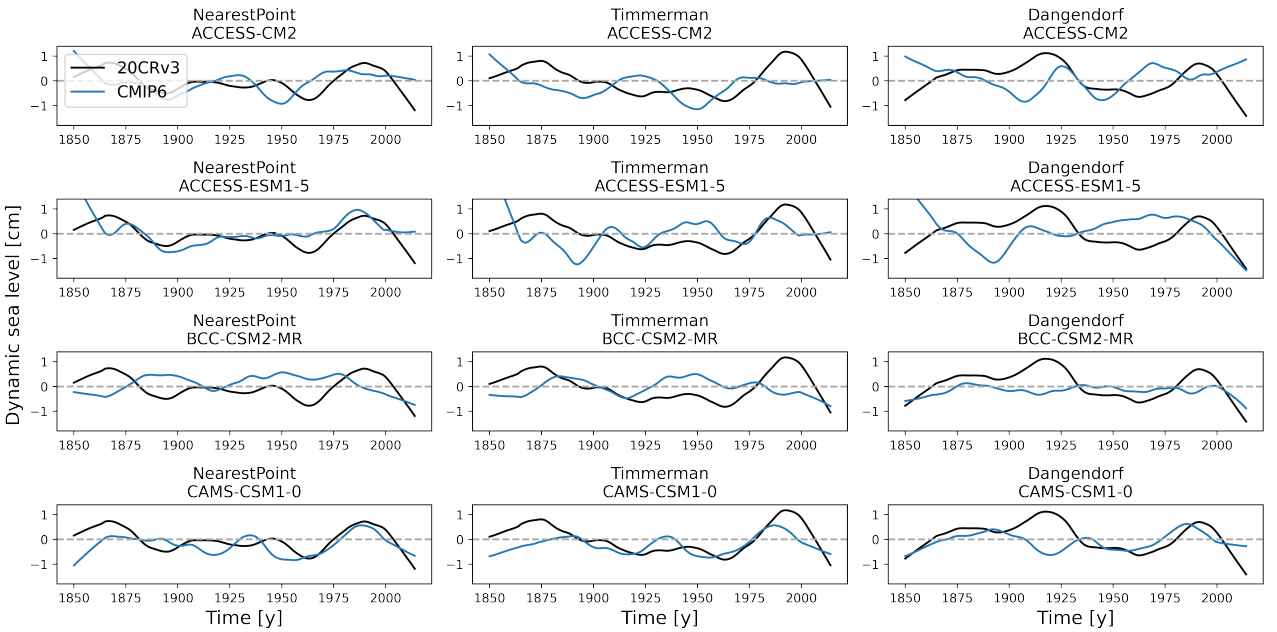

Figure 18: Part 1: Time series of the wind influence on sea-level change resulting from the regression analyses using 20CRv3 and climate model data. Only the time series are shown for the 50% of the climate models that reconstruct the wind influence best compared to the 20CRv3 results.

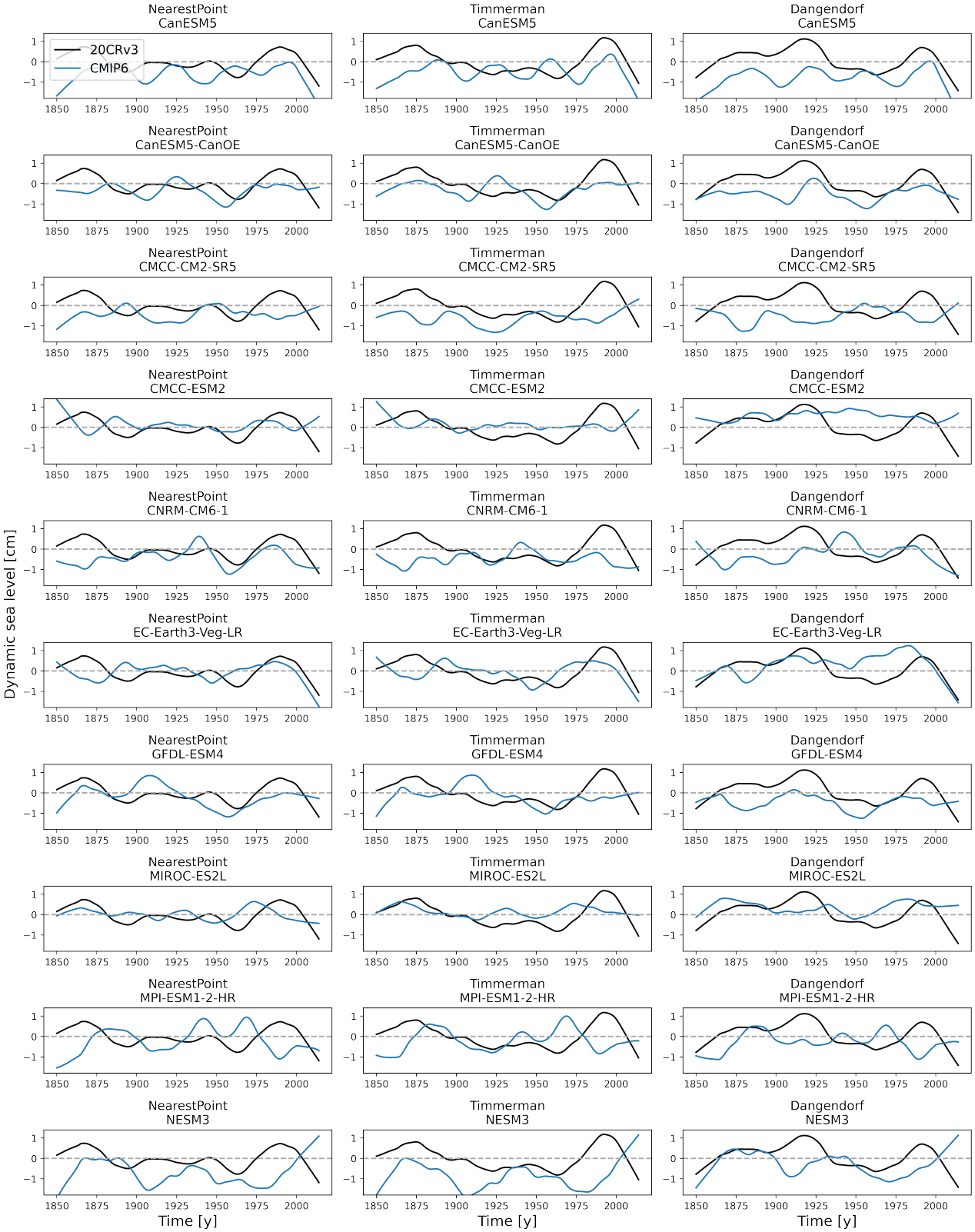

Figure 19: Part 2: Time series of the wind influence on sea-level change resulting from the regression analyses using 20CRv3 and climate model data. Only the time series are shown for the 50% of the climate models that reconstruct the wind influence best compared to the 20CRv3 results.

4.5 Projecting the Wind Influence on Sea-Level Change into the 21st Century

In this final section, we show the results of the wind influence for the 21st century. We project the wind influence using the regression coefficients of the analysis over the historical period using three different climate scenarios: SSP1-RCP2.6, SSP2-RCP4.5, SSP5-RCP8.5. The resulting, smoothed time series for the 6 climate models selected in the previous section are shown in Fig. 20. There are some differences for the different climate models and scenarios but the results for the different regression models are quite similar. All climate models show a continuation of the natural variability of the wind with amplitudes smaller or close to 1 cm. There are no substantial differences in the results for the different scenarios and regression models for most climate models. The linear trends of the wind influence obtained from 2001 to 2100 are shown in Tab. 5. The models ACCESS-ESM1-5, CAMS-CSM1-0, CNRM-CM6-1 and EC-Earth2-Veg-LR have trends close to zero with little difference between the results of the different regression models. The linear trends for the model CanESM5-CanOE are negative, between -0.1 and 0.0 mm/yr and for GFDL-ESM4 trends are largest between 0.0 and 0.4 mm/yr with higher trends for the high-end emission scenario. While most models indicate no significant increase of the wind influence for 2100, at largest an increase of 3 cm for the GFDL-ESM4 climate model using Dangendorf and SSP5-RCP8.5 is found. These results of the trends for the 21st century contradict the results found in [Dangendorf, Wahl, et al. 2014] where a change in long-term wind is found being able to raise sea level in 2100 by 5-6 cm.

Fig. 21 shows the projections of the ensemble of the 50% best-performing climate models. The median and 5th and 95thpercentiles of the climate models are shown with a 10 yr running average applied. From these plots it can be seen that there is no difference in the results of the wind influence for the different scenarios and the different used regression models. These plots show that the natural variability of the wind influence continues throughout the 21st century with an amplitude around 1 cm and no structural change of the wind effect.

The results over the historical period of the climate models CAMS-CSM1-0 and EC-Earth3-Veg-LR is most similar to the observations. From the results of these two models for coming decades, as shown in Fig. 20, the wind influence on sea-level change increases after a drop and is close to zero.

Table 5: Linear trends of the wind influence on sea-level change resulting from the projections for the 21st century. The linear trends are calculated from 2001 to 2100 and have units mm/yr and are reported with an error of one standard deviation.

Model	Scenario	NearestPoint	Timmerman	Dangendorf
ACCESS-ESM1-5	SSP1	0.05 ± 0.03	-0.03 ± 0.04	0.15 ± 0.03
	SSP2	0.03 ± 0.03	0.02 ± 0.04	0.07 ± 0.04
	SSP5	0.02 ± 0.03	-0.02 ± 0.04	0.05 ± 0.03
CAMS-CSM1-0	SSP1	0.02 ± 0.03	0.05 ± 0.03	0.02 ± 0.03
	SSP2	0.04 ± 0.03	0.04 ± 0.03	0.01 ± 0.03
	SSP5	0.10 ± 0.04	0.04 ± 0.04	0.02 ± 0.03
CNRM-CM6-1	SSP1	0.02 ± 0.04	0.04 ± 0.03	0.06 ± 0.03
	SSP2	0.02 ± 0.04	0.04 ± 0.03	0.07 ± 0.03
	SSP5	0.07 ± 0.04	0.06 ± 0.04	0.13 ± 0.03
CanESM5-CanOE	SSP1	-0.06 ± 0.03	-0.05 ± 0.04	-0.04 ± 0.04
	SSP2	-0.09 ± 0.03	-0.09 ± 0.03	-0.09 ± 0.04
	SSP5	-0.01 ± 0.04	-0.06 ± 0.03	-0.05 ± 0.03
EC-Earth3-Veg-lR	SSP1	-0.01 ± 0.03	0.01 ± 0.04	0.04 ± 0.03
	SSP2	-0.03 ± 0.03	-0.03 ± 0.03	-0.01 ± 0.04
	SSP5	0.04 ± 0.03	0.05 ± 0.04	0.06 ± 0.04
GFDL-ESM4	SSP1	0.10 ± 0.07	0.02 ± 0.1	0.23 ± 0.03
	SSP2	0.21 ± 0.06	0.07 ± 0.10	0.27 ± 0.05
	SSP5	0.17 ± 0.06	0.30 ± 0.11	0.32 ± 0.05

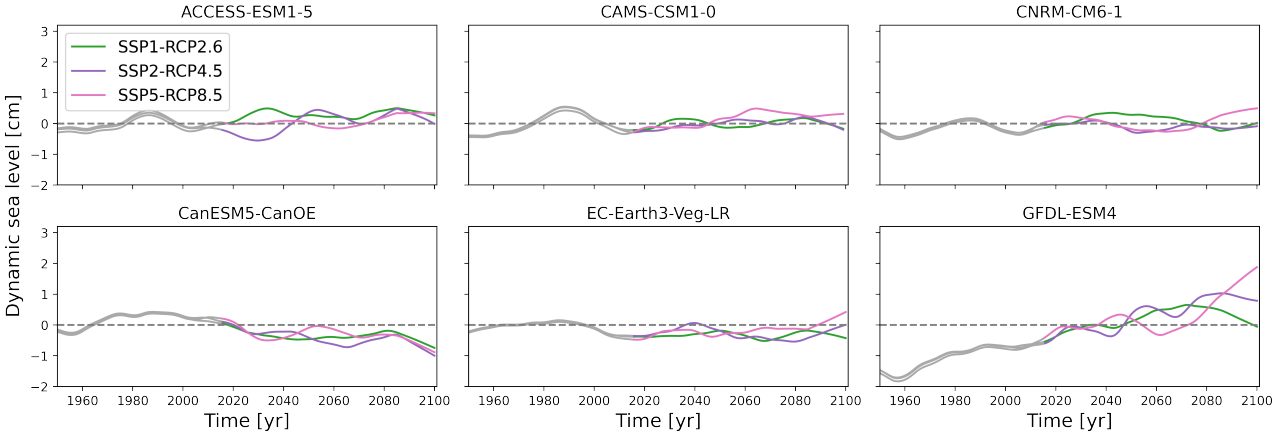

(a) Results for the NearestPoint regression model.

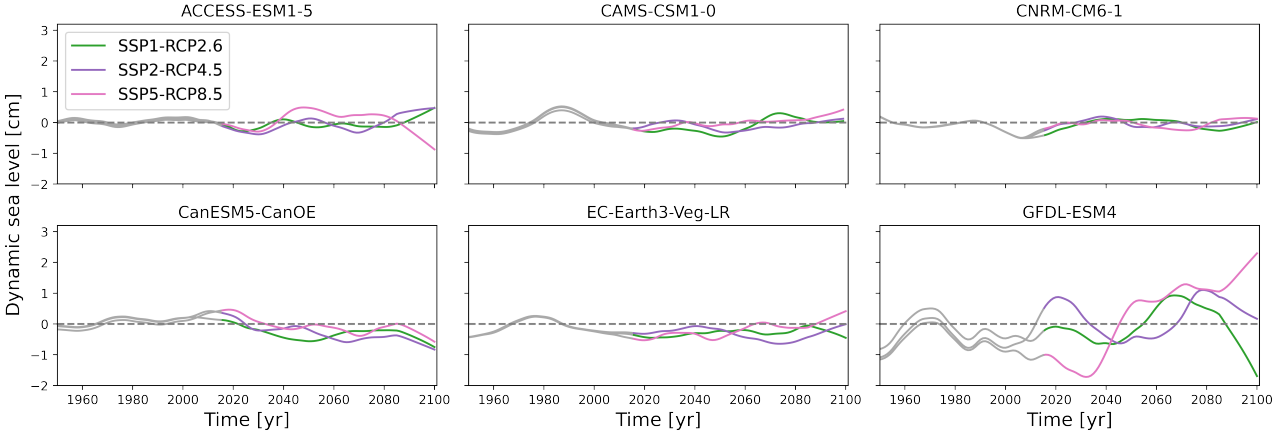

(b) Results for the Timmerman regression model.

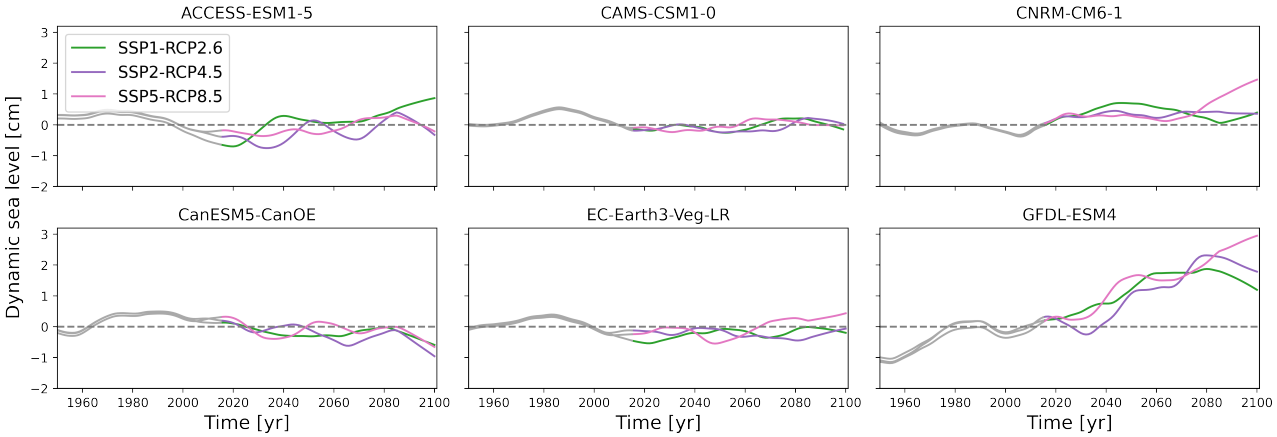

(c) Results for the Dangendorf regression model.

Figure 20: Projections of the wind influence on sea-level change for the 21st century using three climate scenarios.

Figure 21: Projections of the wind influence on dynamic sea-level change for the 21st century of the ensemble of the 50% best-performing climate models. The median and 5th and 95th percentiles of the projections are shown for the NearestPoint, Timmerman and Dangendorf regression models. The projections are obtained for the scenarios SSP1-RCP2.6, SSP2-RCP4.5 and SSP5-RCP8.5. A running average of 10 years has been applied.

5 Conclusions and Discussion

5.1 Conclusions

Now that our results have been presented, we can answer the research questions formulated in the Introduction, Sect. 1.

1. *What was the wind influence on sea-level change along the Dutch coast over the historical period?*
   From our regression analysis using observational sea level data and reanalysis atmospheric data, we find both a structural change of the wind influence on sea-level changes between 0.1 and 0.3 mm/yr over the period from 1836 to 2015 and a solid wind-driven multi-decadal sea-level variability that has an amplitude of 1.0 cm and a period of 40 to 60 years. On decadal time scales, the changes of the wind influence are thus dominated by natural variability. The wind influence increased between about 1960 and 1990, decreased again between about 1990 and 2010 and stabilised over the last decade. When we correct the sea level measurements for this wind effect, we see an acceleration of sea-level rise. The negative trend of the wind influence over recent decades thus played a role in masking an acceleration of sea-level rise along the Dutch coast.

2. *Can we identify large scale drivers of the wind-driven sea-level variability?*
   The multi-decadal wind-driven sea-level variability can be linked to the Atlantic Multidecadal Variability (AMV) and sea surface temperature (SST) in the North Atlantic Ocean. Our results using 20CRv3 data and the Dangendorf regression model indicate that the AMV explains between 35% and 68% of the variance in the wind-driven sea-level variability. However, using 20CRv3 data and the NearestPoint or Timmerman regression model, explained variances are lower, between 0% and 26%. These differences are due to differences in the time series of the wind-driven sea-level variability before 1950. Using ERA5 data, we find that the AMV explains between 50% and 78% of the wind-driven sea-level variability. Though, the period included in this regression analysis only includes one period of the multi-decadal variability of the AMV and wind-driven sea-level variability which lessens the credibility of these results. R^2 values are highest for a lag between 5 and 10 years. For the regression using SST from the North Atlantic Ocean, we find explained variances up to 70% for ocean waters around southern Greenland and Iceland and along the eastern American coast. The wind-driven sea-level variability can thus directly be linked to the SST for these regions in the North Atlantic Ocean. An inverse relationship with the multi-decadal wind variability is found for both the AMV and SST results.

3. *What can be expected of the wind influence for the 21st century?*
   We find that for the 21st century, changes in the wind influence on sea level are driven by natural variability, as was also seen for the historic period. There is no sign of a structural change of the wind influence over the 21st century which contradicts our findings using historical observations. While the wind was able to mask part of the acceleration of sea-level rise over recent decades, this is not expected for coming decades. Therefore, it is expected that an acceleration of sea-level rise will become apparent during the coming decades.

5.2 Discussion

We found that the wind influence on sea-level change using observational data agreed well for the used regression models and reanalysis data after 1950. However, before 1950 there are differences between the time series resulting from the regression models. Especially the Dangendorf regression model departs from the other two. Reanalysis data products can be expected to perform less good further back in time, as less good measurements and no satellite observatory is available. An evaluation of the 20CRv3 data set indeed showed that the performance is less good for the 19$^{\text{th}}$ century compared to the 20$^{\text{th}}$ century and start of the 21$^{\text{st}}$ century [Slivinski et al. 2021]. The Dangendorf regression model uses sea level pressure, whereas the other two models use wind speed. This might cause the difference between their results for the period where the reanalysis data products perform less well; however, at this moment, which variables are better can not be said. Also, there is a difference in the spatial scale of the data retrieved for the different regression models. The Dangendorf model obtains data on a scale of thousands of kilometres; the Timmerman model on a scale of hundreds of kilometres, and the NearestPoint model on a scale of tens of kilometres. Although the 20CRv3 data set is evaluated to perform well on both spatial scales, as described in [Slivinski et al. 2021], there might be a difference for the 19$^{\text{th}}$ century. However, again, on what scale the data performs better is not known. Further knowledge of different aspects of the performance of the 20CRv3 data for the 19$^{\text{th}}$ century are thus essential to get a better understanding of the wind influence for that period. The Timmerman and NearestPoint models use wind measurements and multiply these by their absolute values to obtain wind forcing variables to use in the regression. The Dangendorf model uses a difference of pressure anomalies comparable to the North Atlantic Oscillation (NAO). The difference of these pressure anomalies influences sea level not only through zonal wind stress forcing but also through other mechanisms like the IBE and precipitation [Dangendorf, Wahl, et al. 2014; Tsimplis et al. 2006; Chen et al. 2014]. The Timmerman and NearestPoint models mainly show sea-level changes resulting from wind speed changes. The Dangendorf model can also show sea-level changes resulting from changes in wind direction. These differences between the regression models might drive the differences between their results for the wind influence. As shown in Sect. 4.1, the RMSE and R^2 values indicated that the Timmerman model performed best using the 20CRv3 data. However, this model contains many more explanatory variables. While the LASSO regression does exclude some variables, it still contains double or triple as many explanatory variables depending on the used reanalysis dataset.

The regression analysis between the AMV and the wind-driven sea-level variability showed that the explained variances are highest for the regression using the ERA5 data. However, the ERA5 analysis is performed over a much shorter period, including only one period of the multi-decadal variability which attenuates the credibility of these regression results. Therefore, the results using the 20CRv3 data are important since it covers a period going further back in time. However, for the analysis using 20CRv3 data, we found a difference in the correlation results for the different regression models. While using the Dangendorf model indicates explained variances between 35% and 68%, using the other models results in explained variances between 0% and 26%. These differences are caused by the difference in the time series of the wind influence before 1950, which were described in the previous paragraph. It is thus essential for the study of the influence of the AMV on the wind-driven sea-level variability to have a better understanding of the atmospheric variables before 1950. Our study of the influence of the AMV on the multi-decadal wind-driven sea-level variability showed that the correlation is strongest for a lag between 5 and 10 yr. This implies that an increase of the AMV leads to lower sea levels along the Dutch coast 5 to 10 years later. In Sec. 4.3 we showed that the multi-decadal wind-driven sea-level variability can be directly linked to the SST in some regions of the North Atlantic Ocean. These regions include ocean waters along America's east coast and southern Greenland and Iceland. The wind-driven sea-level variability thus does not seem to relate directly to the AMV but rather to SST changes from certain parts of the North Atlantic Ocean.

An essential difference between the wind influence on sea-level change is the long-term trend that has been found for the results from observations but not for the results from climate model data. This indicates that either the observations are correct and there is a structural wind-driven sea-level change between 0.1 and 0.3 mm/yr or the climate models are correct. The majority indicate that there is no statistically significant change. When the climate models are wrong, this has implications for our projections. If no long-term trend has been observed over the historical period, this trend will also not be present in the projections. An earlier study for the German Bight, using climate model data from CMIP3, found a structural change of the wind effect resulting in a sea-level rise of 3 to 6 cm for 2100 [Dangendorf, Wahl, et al. 2014]. Extending the current study region to the German Bight could show whether the difference in results is caused by the difference in used climate model data or the study region. It might also be that the trend found using observations is a result of natural variability, which is less strong in the climate models. Also, Chapter 8 of KNMI's Klimaatsignaal'21 shows that there have been no significant increases in storm surges due to wind along the Dutch coast and that they do also not show up in the projections [KNMI 2021]. Since sea-level rise along the Dutch coast is expected to accelerate throughout the 21$^{\text{st}}$ century and have increased between 30 to 120 cm by 2100, this structural

wind effect will decrease in relevance over time.

Next to wind forcing also air pressure can have an important effect on annual sea-level changes of 10-30% [Piecuch, Thompson, and Donohue 2016]. Therefore, to understand the wind influence best, it is also essential to understand the pressure influence on sea-level changes. In this analysis, we correct the sea level data for the inverted barometer response before performing the regression analysis as described in Sect. 2.1.1. Uncertainties in the pressure data from the reanalysis data sets lead to uncertainties in this correction [Piecuch, Thompson, and Donohue 2016]. To bypass the uncertainties in the reanalysis data sets, one could analyse the tide gauge surge data and use harmonic analysis to correct these for sea-level changes due to tidal forces.

In the analysis, time series are detrended by removing the linear trend. However, some time series, like sea surface temperatures, include an accelerating signal resulting from global warming. In such a case, using a linear detrending method might cause spurious correlations in the regression analysis.

Acknowledgements

During this project, I have been supported by many amazing people. Due to the strange circumstances, which caused me to stay home most of the time, I am even more grateful for the support given. First, I would like to thank my primary supervisor Dr. Dewi Le Bars, whose input is fundamental for this project. Thank you for the continuous support, valuable feedback and joyful conversations and for giving me the fantastic opportunity of doing this project at KNMI. Our long and frequent online meetings have been very important for my research and motivation. Second, I would also like to thank my other supervisor Prof. Dr. Roderik van de Wal for his valuable insights and support when needed.

Also, a huge thanks to everyone from the Sea-Level Team of KNMI. They welcomed me into their group, spent a great time discussing my results and gave me helpful insights. I have also very much enjoyed our long coffee breaks and lunch walks. A special thanks for André for kindly offering me the detrended AMV data sets and giving feedback on my thesis. I am very grateful for and looking forward to continuing to work in the team.

At last, I want to thank my family, friends, fellow master students and others I have met at KNMI, for their support and having a lot of good times. A special thanks to Ina, Marta, Sophie, Lena and Neha for being the best study friends, to my parents and sister for relaxed weekends at home and to Bohdy for the amazing walks to clear my head.

References to Data

Hersbach, H., Bell, B., and Berrisford, P. (2021). *ERA5 monthly averaged data on single levels from 1979 to present. Copernicus Climate Change Service (C3S) Climate Data Store (CDS).* Data retrieved on 1 April 2021 from , `https://cds.climate.copernicus.eu/cdsapp#!/dataset/reanalysis-era5-single-levels-monthly-means?tab=overview` and `https://cds.climate.copernicus.eu/cdsapp#!/dataset/reanalysis-era5-pressure-levels-monthly-means-preliminary-back-extension?tab=overview`.

Hirahara, S., Ishii, M., and Fukuda, Y. (2014). "Centennial-scale sea surface temperature analysis and its uncertainty". In: *Journal of Climate* 27.1, pp. 57–75.

PSL, NOAA/OAR/ESRL (2021). *Twentieth Century Reanalysis V3 data.* Data retrieved on 1 April 2021 from , `https://psl.noaa.gov/data/gridded/data.20thC_ReanV3.monolevel.html#caveat`.

PSMSL (2021). *Tide Gauge Data. Permanent Service for Mean Sea Level.* Data retrieved on 1 November 2021 from , `http://www.psmsl.org/data/obtaining/`.

Rayner, N. A. A., de Parker, E., Horton, E. B., Folland, C. K., Alexander, L. V., Rowell, D. P., Kent, E. C., and Kaplan, A. (2003). "Global analyses of sea surface temperature, sea ice, and night marine air temperature since the late nineteenth century". In: *Journal of Geophysical Research: Atmospheres* 108.D14.

References to Papers

Baart, F., van Gelder, P. H. A. J. M., de Ronde, J., van Koningsveld, M., and Wouters, B. (2012). "The effect of the 18.6-year lunar nodal cycle on regional sea-level rise estimates". In: *Journal of Coastal research* 28.2, pp. 511–516.

Baart, F., Rongen, G., Hijma, M., Kooi, H., de Winter, R., and Nicolai, R. (2019). "Zeespiegelmonitor 2018. De stand van zaken rond de zeespiegelstijging langs de Nederlandse kust". In.

Babadi, B. and Brown, E. N. (2014). "A review of multitaper spectral analysis". In: *IEEE Transactions on Biomedical Engineering* 61.5, pp. 1555–1564.

Bell, B., Hersbach, H., Simmons, A., Berrisford, P., Dahlgren, P., Horányi, A., Muñoz-Sabater, J., Nicolas, J., Radu, R., Schepers, D., et al. (2021). "The ERA5 global reanalysis: Preliminary extension to 1950". In: *Quarterly Journal of the Royal Meteorological Society* 147.741, pp. 4186–4227.

Chen, Xinping, Dangendorf, Sönke, Narayan, Nikesh, O'Driscoll, Kieran, Tsimplis, Michael N, Su, Jian, Mayer, Bernhard, and Pohlmann, Thomas (2014). "On sea level change in the North Sea influenced by the North Atlantic Oscillation: local and remote steric effects". In: *Estuarine, Coastal and Shelf Science* 151, pp. 186–195.

Church, J. A. and White, N. J. (2011). "Sea-level rise from the late 19th to the early 21st century". In: *Surveys in geophysics* 32.4, pp. 585–602.

Dangendorf, S., Hay, C., Calafat, F. M., Marcos, M., Piecuch, C. G., Berk, K., and Jensen, J. (2019). "Persistent acceleration in global sea-level rise since the 1960s". In: *Nature Climate Change* 9.9, pp. 705–710.

Dangendorf, S., Marcos, M., Wöppelmann, G., Conrad, C. P., Frederikse, T., and Riva, R. (2017). "Reassessment of 20th century global mean sea level rise". In: *Proceedings of the National Academy of Sciences* 114.23, pp. 5946–5951.

Dangendorf, S., Wahl, T., Nilson, E., Klein, B., and Jensen, J. (2014). "A new atmospheric proxy for sea level variability in the southeastern North Sea: observations and future ensemble projections". In: *Climate dynamics* 43.1, pp. 447–467.

Douglas, B. C. (1992). "Global sea level acceleration". In: *Journal of Geophysical Research: Oceans* 97.C8, pp. 12699–12706.

Fox-Kemper, B., Hewitt, H. T., Xiao, C., Aðalgeirsdóttir, G., Drijfhout, S. S., Edwards, T. L., Golledge, N. R., Hemer., M., Kopp, R. E., Krinner, G., Mix, A., Notz, D., Nowicki, S., Nurhati, I. S., Ruiz, L., Sallée, J-B, Slangen, A. B. A., and Yu, Y. (2021). "Ocean, Cryosphere and Sea Level Change. In: Climate Change 2021: The Physical Science Basis. Contribution of Working Group I to the Sixth Assessment Report of the Intergovernmental Panel on Climate Change". In: *Cambridge University Press. In Press.*

Frederikse, T., Landerer, F., Caron, L., Adhikari, S., Parkes, D., Humphrey, V. W., Dangendorf, S., Hogarth, P., Zanna, L., Cheng, L., et al. (2020). "The causes of sea-level rise since 1900". In: *Nature* 584.7821, pp. 393–397.

Gehrels, W. R. and Woodworth, P. L. (2013). "When did modern rates of sea-level rise start?" In: *Global and Planetary Change* 100, pp. 263–277.

Heij, C., de Boer, P., Franses, P. H., Kloek, T., and van Dijk, H. K. (2004). *Econometric Methods with Aplications in Business and Economics.* Oxford University Press.

Hermans, T. H. J., Bars, D. Le, Katsman, C. A., Camargo, C. M. L., Gerkemam, T., Calafat, F. M., Tinker, J., and Slangen, A. B. A. (2020). "Drivers of interannual sea level variability on the northwestern European shelf". In: *Journal of Geophysical Research: Oceans* 125.10, e2020JC016325.

Hersbach, H., Bell, B., Berrisford, P., Hirahara, S., Horányi, A., Muñoz-Sabater, J., Nicolas, J., Peubey, C., Radu, R., Schepers, D., et al. (2020). "The ERA5 global reanalysis". In: *Quarterly Journal of the Royal Meteorological Society* 146.730, pp. 1999–2049.

Hinkel, J., Lincke, D., Vafeidis, A. T., Perrette, M., Nicholls, R. J., Tol, R. S. J., Marzeion, B., Fettweis, X., Ionescu, C., and Levermann, A. (2014). "Coastal flood damage and adaptation costs under 21st century sea-level rise". In: *Proceedings of the National Academy of Sciences* 111.9, pp. 3292–3297.

Holgate, S. J., Matthews, A., Woodworth, P. L., Rickards, L. J., Tamisiea, M. E., Bradshaw, E., Foden, P. R., Gordon, K. M., Jevrejeva, S., and Pugh, J. (2013). "New data systems and products at the permanent service for mean sea level". In: *Journal of Coastal Research* 29.3, pp. 493–504.

Huang, B., Thorne, P. W., Banzon, V. F., Boyer, T., Chepurin, G., Lawrimore, J. H., Menne, M. J., Smith, T. M., Vose, R. S., and Zhang, H-M (2017). "Extended reconstructed sea surface temperature, version 5 (ERSSTv5): upgrades, validations, and intercomparisons". In: *Journal of Climate* 30.20, pp. 8179–8205.

Jeffreys, H. (1916). "Causes contributory to the annual variation of latitude". In: *Monthly Weather Review* 44.6, pp. 337–337.

Jüling, A., von der Heydt, A., and Dijkstra, H. A. (2021). "Effects of strongly eddying oceans on multidecadal climate variability in the Community Earth System Model". In: *Ocean Science* 17.5, pp. 1251–1271.

Kirwan, M. L. and Megonigal, J. P. (2013). "Tidal wetland stability in the face of human impacts and sea-level rise". In: *Nature* 504.7478, pp. 53–60.

KNMI (2021). *Klimaatsignaal'21: hoe het klimaat in Nederland snel verandert.*

Van Koningsveld, M., Mulder, J. P. M., Stive, M. J. F., van der Valk, L., and van der Weck, A. W. (2008). "Living with sea-level rise and climate change: a case study of the Netherlands". In: *Journal of coastal research* 24.2, pp. 367–379.

Kopp, R. E., Kemp, A. C., Bittermann, K., Horton, B. P., Donnelly, J. P., Gehrels, W. R., Hay, C. C., Mitrovica, J. X., Morrow, E. D., and Rahmstorf, S. (2016). "Temperature-driven global sea-level variability in the Common Era". In: *Proceedings of the National Academy of Sciences* 113.11, E1434–E1441.

Meyssignac, B. and Cazenave, A. (2012). "Sea level: a review of present-day and recent-past changes and variability". In: *Journal of Geodynamics* 58, pp. 96–109.

Meyssignac, B., Slangen, A. B. A., Melet, A., Church, J. A., Fettweis, X., Marzeion, B., Agosta, C., Ligtenberg, S. R. M., Spada, G., Richter, K., et al. (2017). "Evaluating model simulations of twentieth-century sea-level rise. Part II: Regional sea-level changes". In: *Journal of Climate* 30.21, pp. 8565–8593.

Nauels, A., Rogelj, J., Schleussner, C-F, and Mengel, M. Meinshausenand M. (2017). "Linking sea level rise and socioeconomic indicators under the Shared Socioeconomic Pathways". In: *Environmental Research Letters* 12.11, p. 114002.

Nicholls, R. J., Hanson, S., Lowe, J. A., Slangen, A. B. A., Wahl, T., Hinkel, J., and Long, A. J. (2019). "Sea-level scenarios for evaluating coastal impacts and adaptation responses". In: *AGU Fall Meeting Abstracts.* Vol. 2019, OS31D–1777.

Piecuch, C. G., Thompson, P. R., and Donohue, K. A. (2016). "Air pressure effects on sea level changes during the twentieth century". In: *Journal of Geophysical Research: Oceans* 121.10, pp. 7917–7930.

Ray, R. D. and Douglas, B. C. (2011). "Experiments in reconstructing twentieth-century sea levels". In: *Progress in Oceanography* 91.4, pp. 496–515.

Slangen, A. B. A., Church, J. A., Agosta, C., Fettweis, X., Marzeion, B., and Richter, K. (2016). "Anthropogenic forcing dominates global mean sea-level rise since 1970". In: *Nature Climate Change* 6.7, pp. 701–705.

Slangen, A. B. A., van de Wal, R. S. W., Wada, Y., and Vermeersen, L. L. A. (2014). "Comparing tide gauge observations to regional patterns of sea-level change (1961–2003)". In: *Earth System Dynamics* 5.1, pp. 243–255.

Slivinski, L. C., Compo, G. P., Sardeshmukh, P. D., Whitaker, J. S., McColl, C., Allan, R. J., Brohan, P., Yin, X., Smith, C. A., Spencer, L. J., et al. (2021). "An evaluation of the performance of the twentieth century reanalysis version 3". In: *Journal of Climate* 34.4, pp. 1417–1438.

Stammer, D. and Höttemann, S. (2008). "Response of regional sea level to atmospheric pressure loading in a climate change scenario". In: *Journal of Climate* 21.10, pp. 2093–2101.

Thomson, D. J. (1982). "Spectrum estimation and harmonic analysis". In: *Proceedings of the IEEE* 70.9, pp. 1055–1096.

Thomson, R. E. and Emery, W. J. (2014). *Data analysis methods in physical oceanography.* Newnes.

Tibshirani, R. (1996). "Regression shrinkage and selection via the lasso". In: *Journal of the Royal Statistical Society: Series B (Methodological)* 58.1, pp. 267–288.

Timmerman, H. (1975). "On the importance of atmospheric pressure gradients for the generation of external surges in the North Sea." In: *Deutsche Hydrographische Zeitschrift* 28.2, pp. 62–71.

Tranmer, M. and Elliot, M. (2008). "Multiple linear regression". In: *The Cathie Marsh Centre for Census and Survey Research (CCSR)* 5.5, pp. 1–5.

Tsimplis, M. N., Shaw, A. G. P., Flather, R. A., and Woolf, D. K. (2006). "The influence of the North Atlantic Oscillation on the sea-level around the northern European coasts reconsidered: the thermosteric effects".

In: *Philosophical Transactions of the Royal Society A: Mathematical, Physical and Engineering Sciences* 364.1841, pp. 845–856.

Vermeersen, B. L. A., Slangen, A. B. A., Gerkema, T., Baart, F., Cohen, K. M., Dangendorf, S., Duran-Matute, M., Frederikse, T., Grinsted, A., Hijma, M. P., et al. (2018). "Sea-level change in the Dutch Wadden Sea". In: *Netherlands Journal of Geosciences* 97.3, pp. 79–127.

Van Vuuren, D. P., Edmonds, J., Kainuma, M., Riahi, K., Thomson, A., Hibbard, K., Hurt, G. C., Kram, T., Krey, V., Lamarque, J, et al. (2011). "The representative concentration pathways: an overview". In: *Climatic change* 109.1, pp. 5–31.

Woodworth, P. L. (2012). "A note on the nodal tide in sea level records". In: *Journal of Coastal Research* 28.2, pp. 316–323.

Wöppelmann, G., Letetrel, C., Santamaria, A., Bouin, M-N, Collilieux, X., Altamimi, Z., Williams, S. D. P., and Miguez, B. M. (2009). "Rates of sea-level change over the past century in a geocentric reference frame". In: *Geophysical Research Letters* 36.12.

Wunsch, C. and Stammer, D. (1997). "Atmospheric loading and the oceanic "inverted barometer" effect". In: *Reviews of Geophysics* 35.1, pp. 79–107.

Yiou, P., Baert, E., and Loutre, M-F (1996). "Spectral analysis of climate data". In: *Surveys in Geophysics* 17.6, pp. 619–663.

A The Wind Influence on Sea-Level Change using Observations from Individual Tide Gauge Stations

The regression analysis studying the wind influence on sea-level change using the NearestPoint, Timmerman and Dangendorf regression models is not only performed for the average of the 6 tide gauge stations but also for each individual tide gauge station. The resulting time series of the wind influence, smoothed with a 31-year window are shown in Fig. 22. The resulting linear trends obtained over 39-year periods are shown in Fig. 23.

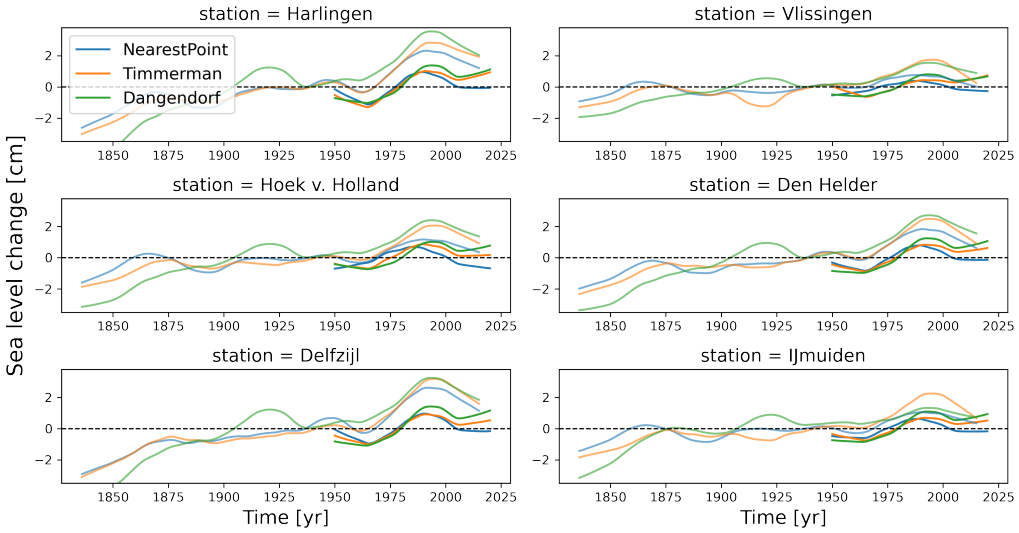

Figure 22: Annual time series of the wind influence on sea level changes smoothed using a 31-year window. The 20CRv3 results are the transparent lines and the ERA5 results are the bold lines.

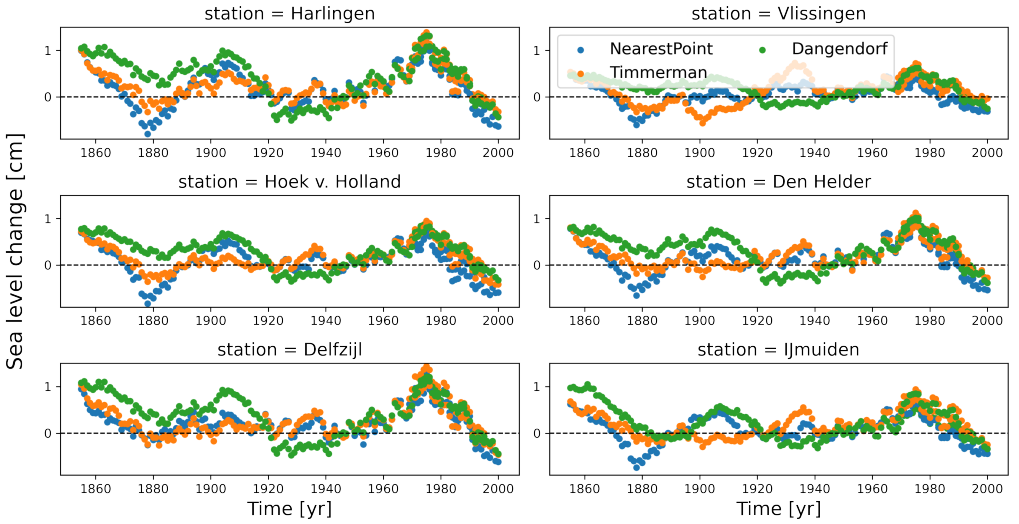

Figure 23: Annual time series of the wind influence on sea level changes smoothed using a 31-year window. The 20CRv3 results are the transparent lines and the ERA5 results are the bold lines.

B The Influence of the AMV on Wind-Driven Sea-Level Variability

B.1 Analysis over the Period from 1950 to 2015

The difference in the explained variances resulting from the regression between ERA5 and 20CRv3 data might be explained from the fact that a different time period is analysed. To check this, the regression analysis is also performed using both ERA5 and 20CRv3 data from 1950 to 2015. The resulting R^2 values are shown in Fig. 24. The results are very consistent for the analyses using different data sets and regression models. Again, the explained variances are highest for a lag between 5 and 15 years. For such lags the explained variances are very high reaching between 86% and 96%. We also found very high variances for the analysis using ERA5 data over the period from 1950 to 2018.

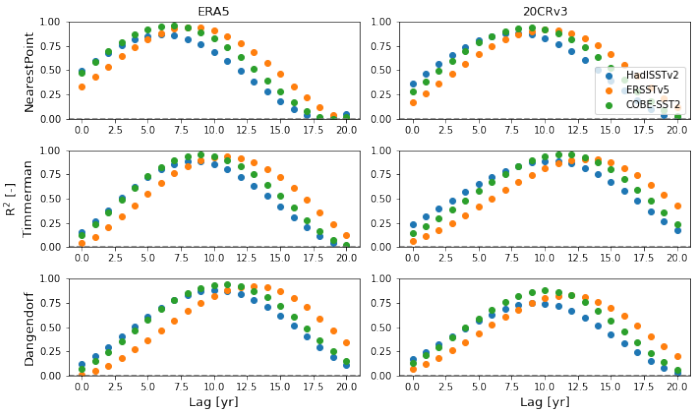

Figure 24: Plots of the R^2 results of the regression between detrended and smoothed AMV data and the wind-driven sea-level variability over the period from 1950 to 2015.

B.2 Analysis using Smoothing Functions with a Window of 11 and 21 Years

The analysis between the AMV and wind-driven sea-level variability is performed using detrended and smoothed functions. Because we studied the multidecadal variability we used a smoothing function with a 31 yr window. This resulted in time series showing the interdecadal variability but no interannual variability. To check the influence of the window used for smoothing the time series, the analysis is repeated using windows of 11 and 21 years. The R^2 values resulting from these analyses are shown in Fig. 25. These results show that the explained variances are still highest for a window above 5 years. However, using a smaller window leads to smaller lags having the highest explained variances. This becomes clear when we study for each lag, for how many analysis this lag had the highest explained variance. These results are shown in the bar plots in Fig. 26.

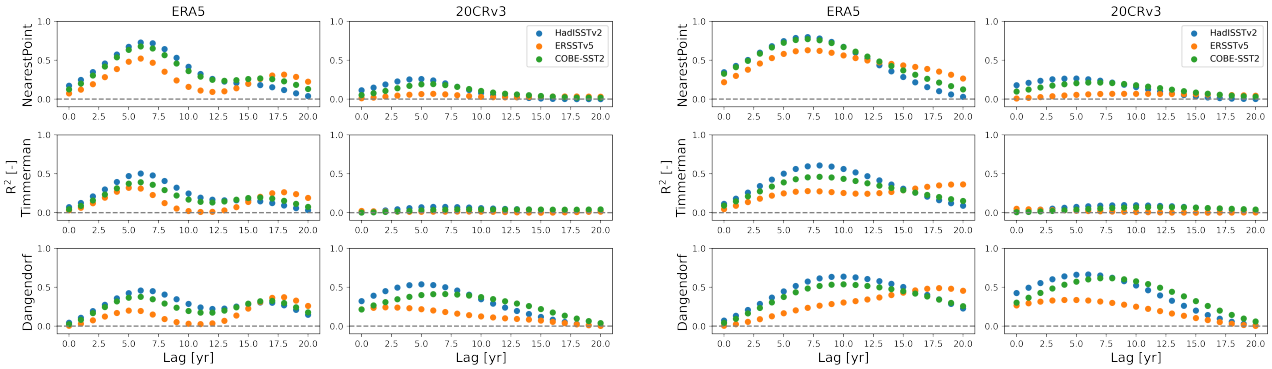

(a) Results of the analysis using a window of 11 years.

(b) Results of the analysis using a window of 21 years.

Figure 25: Plots of the R^2 results of the regression between detrended and smoothed AMV data and the wind-driven sea-level variability using a window of 11 or 21 years to smooth the time series.

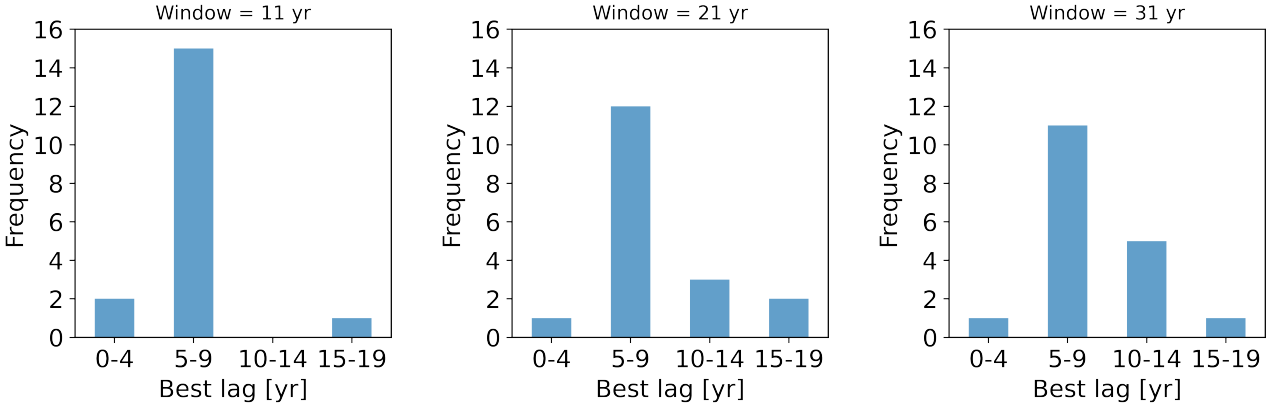

Figure 26: Bar plots showing for how many analyses the lag with the highest explained variance lies in a specific range of lags for the regression analysis performed using time series smoothed with a 11, 21 or 31 yr window.

C The Influence of SST on Wind-Driven Sea-Level Variability using SKT data

The study of the influence of SST on wind-driven sea-level variability is also performed using 20CRv3 SKT data. The resulting R^2 values and regression coefficients are shown in Fig. 27. There are no substantial differences to the results presented in Sec. 4.3.

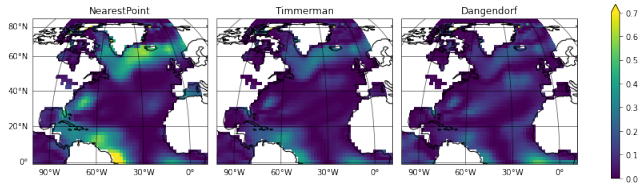

(a) Coefficients of determination resulting from the regression with ERA5 reanalysis data.

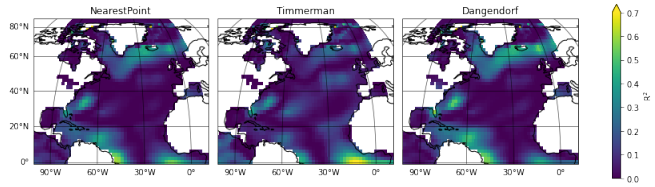

(b) Coefficients of determination resulting from the regression with 20CRv3 reanalysis data.

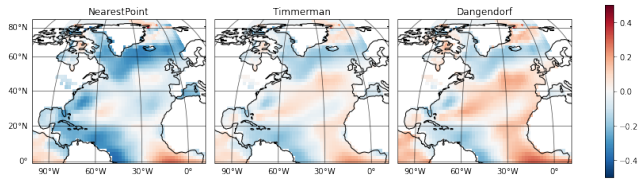

(c) Regression coefficient resulting from the regression with ERA5 reanalysis data.

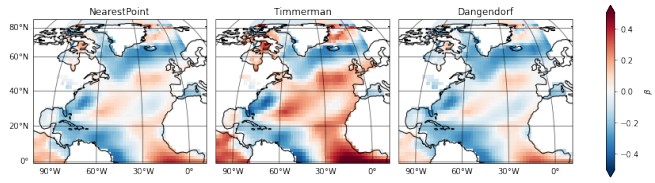

(d) Regression coefficient resulting from the regression with 20CRv3 reanalysis data.

Figure 27: Maps showing the results of the regression between SKT and wind-driven sea-level variability using 20CRv3 reanalysis SKT data.

D The CMIP6 climate models

The CMIP6 climate models used in this study are listed in Tab. 6. The names in bold are the 50% of the climate models that are best at reconstructing the wind influence on sea-level changes.

Table 6: Information about the 28 Climate Models (CMIP6) used in the analysis. The names in bold are the 50% of the models that are best at reconstructing the wind influence on sea-level changes.

Model	Institute, Country
ACCESS-CM2	Commonwealth Scientific and Industrial Research Organisation, Australia
ACCESS-ESM1.5	Commonwealth Scientific and Industrial Research Organisation, Australia
BCC-CSM2-MR	Beijing Climate Center, China
CAMS-CSM1-0	Chinese Academy of Meteorological Sciences, China
CAS-ESM2-0	Chinese Academy of Sciences, China
CMCC-CM2-SR5	Euro-Mediterranean Centre on Climate Change, Italy
CMCC-ESM2	Euro-Mediterranean Centre on Climate Change, Italy
CNRM-CM6-1	National Centre for Meteorological Research, France
CNRM-ESM2-1	National Centre for Meteorological Research, France
CanESM5	Canadian Centre for Climate Modelling and Analysis, Canada
CanESM5-CanOE	Canadian Centre for Climate Modelling and Analysis, Canada
EC-Earth3	Consortium of 30 institutes from 12 European countries
EC-Earth3-Veg	Consortium of 30 institutes from 12 European countries
EC-Earth3-Veg-LR	Consortium of 30 institutes from 12 European countries
GFDL-ESM4	Geophysical Fluid Dynamics Laboratory, United States
GISS-E2-1-G	NASA Goddard Institute for Space Studies, United States
HadGEM3-GC31-LL	Met Office Hadley Centre, United Kingdom
HadGEM3-GC31-MM	Met Office Hadley Centre, United Kingdom
INM-CM4-8	Institute of Numerical Mathematics, Russia
INM-CM5-0	Institute of Numerical Mathematics, Russia
IPSL-CM6A-LR	Institut Pierre-Simon Laplace, France
MIROC-ES2L	Technology, Atmosphere and Ocean Research Institute, Japan
MIROC6	Technology, Atmosphere and Ocean Research Institute, Japa
MPI-ESM1-2-HR	Max Planck Institute for Meteorology, Germany
MPI-ESM1-2-LR	Max Planck Institute for Meteorology, Germany
MRI-ESM2-0'	Meteorological Research Institute, Japan
NESM3	Nanjing University of Information Science and Technology, China
UKESM1-0-LL	UK Centre for Ecology and Hydrology, United Kingdom

E Python Code

The code used in this thesis project can be found at: https://github.com/iris-keizer/Thesis-KNMI